

Impact of Channel Aging on Dual-Function Radar-Communication Systems: Performance Analysis and Resource Allocation

Jie Chen, *Member, IEEE*, Xianbin Wang, *Fellow, IEEE*, and Ying-Chang Liang, *Fellow, IEEE*

Abstract—In conventional dual-function radar-communication (DFRC) systems, the radar and communication channels are routinely estimated at fixed time intervals based on their worst-case operation scenarios. Such situation-agnostic repeated estimations cause significant training overhead and dramatically degrade the system performance, especially for applications with dynamic sensing/communication demands and limited radio resources. In this paper, we leverage the channel aging characteristics to reduce training overhead and to design a situation-dependent channel re-estimation interval optimization-based resource allocation for performance improvement in a multi-target tracking DFRC system. Specifically, we exploit the channel temporal correlation to predict radar and communication channels for reducing the need of training preamble retransmission. Then, we characterize the channel aging effects on the Cramer-Rao lower bounds (CRLBs) for radar tracking performance analysis and achievable rates with maximum ratio transmission (MRT) and zero-forcing (ZF) transmit beamforming for communication performance analysis. In particular, the aged CRLBs and achievable rates are derived as closed-form expressions with respect to the channel aging time, bandwidth, and power. Based on the analyzed results, we optimize these factors to maximize the average total aged achievable rate subject to individual target tracking precision demand, communication rate requirement, and other practical constraints. Since the formulated problem belongs to a non-convex problem, we develop an efficient one-dimensional search based optimization algorithm to obtain its suboptimal solutions. Finally, simulation results are presented to validate the correctness of the derived theoretical results and the effectiveness of the proposed allocation scheme.

Index Terms—Dual-function radar-communication, channel aging, performance analysis, resource allocation.

I. INTRODUCTION

Dual-function radar-communication (DFRC) system has emerged as a promising paradigm in the future generation of wireless systems and networks, particularly in 5G beyond and 6G [1]–[3]. Due to its capability of fulfilling the stringent sensing and transmission demands concurrently, many new use cases, such as augmented/virtual reality, intelligent transportation, and smart manufacturing, can be supported by DFRC. In general, a DFRC system is a jointly designed coexistence system, which integrates both radar sensing and communication functions into a unified physical platform by enabling the shared use of signal waveforms, hardware, and

radio resources. Given its many advantages and promising potentials, the DFRC system has been under intensive investigation in industrial and academic communities.

Due to the perpetual radio resource constraint, efficient radio resource sharing between sensing and communication in DFRC plays a critical role in the system design to achieve desired performance trade-off between concurrent functions [4]. In general, existing research on resource sharing designs in DFRC systems may be classified into three categories, i.e., communication-centric based schemes [5]–[11], sensing-centric based schemes [12]–[18], joint-centric based schemes [19]–[21]. Specifically, for the communication-centric based schemes, the radio resources were allocated to optimize the communication performance metrics, e.g., energy efficiency [5], outage probability [6], bit error rate (BER) [7], and achievable minimum/sum/secret rates [8]–[11], while satisfying the desired radar performance demands. As for sensing-centric based schemes, the resource allocation was investigated to optimize the sensing performance metrics, e.g., desired sensing beam-pattern [12], radar detection probability [13]–[15], and estimation accuracy including mean squared error [16] and Cramer-Rao lower bound (CRLB) [17], [18], subject to the communication performance requirements. For the joint-centric based schemes, the weighted objective of communication and radar was considered, e.g., in [19], the weighted mutual information for sensing and communication was optimized considering the impacts of training overhead and channel estimation error; in [20], the weighted sum of radar CRLB and communication distortion minimum mean square error (MMSE) was optimized by designing an adaptive virtual transmit signal waveform; and in [21], the sum of power consumption for radar and communication is minimized by joint optimizing active and passive beamforming in an IRS-aided DFRC system.

Furthermore, the above studies [5]–[21] focus on sensing-communication performance trade-off in a single transmission block scenario, which cannot be applied to target tracking scenarios with multiple transmission blocks. In fact, target tracking, an essential task, has been intensively studied during the past decades [22]–[27]. Specifically, for target tracking designs in conventional radar systems [22]–[24], the multi-beam resource and power allocation were studied in [22] and [23], respectively, to minimize the maximum Bayesian CRLB among multiple targets, and the joint power and bandwidth allocation was studied in [24] to minimize the weighted posterior CRLB. As for target tracking designs in DFRC

J. Chen and X. Wang are with the Department of Electrical and Computer Engineering, Western University, London, ON N6A 5B9, Canada (e-mails: chenjie.ay@gmail.com, xianbin.wang@uwo.ca). Y.-C. Liang is with Institute for Infocomm Research (I²R), Agency for Science, Technology and Research (A*STAR), Singapore 138632 (e-mail: liangyc@ieee.org).

systems [25]–[27], the radar ranging method was applied to reduce the training overhead of beam alignment in [25], where the cost-benefit trade-off through time allocation between radar and communication modes was analyzed under the IEEE 802.11ad protocol. Then, the message passing [26], extended Kalman filtering [27], and deep learning [28] methods are proposed to estimate/predict the target kinematic parameters, which are further applied to guide resource allocation for communication performance enhancement.

However, most studies in [5]–[29] are designed to routinely estimate communication channel state information (CSI) or radar sensing information (e.g., target mobility/position) at each fixed time interval. Such estimation interval is designed based on the worst-case scenario among all users without considering the specific channel situation and sensing/communication demands, thus causing redundancy and significant training overhead. In fact, the practical sensing/communication channels are time-correlated due to the target/user motion continuity [30]. Such correlations can be explored to predict sensing information and communication CSI [31]. This way, the re-estimation time interval could be increased based on the specific demands, thus reducing training overhead and improving resource utilization efficiency. Since such time correlations become weaker with a longer time interval, the prediction accuracies for sensing information and communication CSI decrease with time, also called channel aging effect.

Investigating channel aging effect and optimizing channel re-estimation time interval to reduce training overhead have been studied in communication systems [32]–[36]. Specifically, for single-user multi-input multi-output (MIMO) cases [32], the effect of channel aging on the system throughput was characterized and the maximum training time interval was derived based on the minimum throughput condition. As for multi-user MIMO cases [33]–[35], the sum rate with the aged CSI was evaluated in [33], [34] with considering the time allocation trade-off between training overhead and data transmission. In [35], an intermittent channel estimation scheme was proposed to reduce the training overhead, and the total throughput was maximized by optimizing training time interval for each user. Moreover, for cell-free MIMO cases [36], the spectral efficiencies (SEs) were derived in uplink and downlink transmissions, and the source block length was designed to mitigate the negative effect of channel aging on SE. Despite the significant benefits of investigating channel aging in communication systems, to the best of our knowledge, there is no study considering channel aging in DFRC systems, where the radar-communication performance analysis and resource allocation design is still an open problem.

Motivated by the above reasons, in this paper, we characterize the channel aging effects on the radar-communication performances and apply them to design a situation-dependent resource allocation scheme for a downlink multi-target tracking DFRC system, in which a full-duplex base station (BS) concurrently communicates with multiple communication users and tracks multiple targets. This system is operated with a novel frame structure consisting of multiple fading blocks to support radar target tracking, communication channel estimation, and

information transmission. Besides, the mobility information of targets and CSI of communication users are estimated in the first block by transmitting training preambles, then predicted in the remaining blocks by leveraging channel aging characteristics without repeated training preamble transmission. Then, resource utilization efficiency can be improved by designing a resource allocation scheme and optimizing channel re-estimation interval with considering the specific radar and communication demands. Finally, to highlight the contributions of this paper, we summarize the paper as follows:

- To the best of our knowledge, it is the first time to characterize the channel aging effects for the DFRC system. Specifically, we characterize the channel aging effects on the tracking performance (i.e., the CRLBs of the predicated mobility information) and the communication performance (i.e., the achievable rates with the predicated CSI under maximum ratio transmission (MRT) and zero-forcing (ZF) transmit beamforming). In particular, the aged CRLBs and achievable rates are derived as closed-form expressions with respect to the allocated bandwidth and power resource and channel aging time. Moreover, to intuitively understand channel aging effects, we propose an approximation method to simplify the derived CRLB expressions and provide the asymptotic analysis of the achievable rate with respect to the transmit power.
- Based on the derived aged tracking and communication performances, a situation-dependent joint channel re-estimation interval together with other radio resource allocation scheme is proposed for system training overhead reduction and performance improvement. Particularly, we formulate an average total aged achievable rate maximization problem subject to individual tracking precision demand, customized communication rate requirement, and other practical constraints. Since the formulated problem belongs to a non-convex mixed integer nonlinear programming (MINLP) problem, an efficient one-dimensional search based optimization algorithm is developed to obtain its suboptimal solutions.
- Simulation results show that the simulated CRLBs and achievable rates can approach the derived theoretical results. Besides, the performance of the proposed algorithm is close to the upper bound performance and is significantly superior to other benchmarks.

The rest of this paper is organized as follows. Section II presents the multi-target/-user DFRC system model. Section III introduces radar and communication channel estimation algorithms and then characterizes the channel aging effects on the tracking and communication performances. Then, Section IV exploits the characterized results to study the average total aged achievable rate maximization problem and provides the corresponding efficient solutions. Finally, Section V provides simulation results and Section VI concludes the paper.

Notation: We use \mathbb{N} and \mathbf{I}_M to denote the set of natural numbers and the M -by- M identity matrix, respectively. We use $\mathbb{E}(\cdot)$ and $\text{var}(\cdot)$ to denote the expectation and variance of the variable, respectively, and use $\text{diag}(\cdot)$ to return a square diagonal matrix with the corresponding elements of

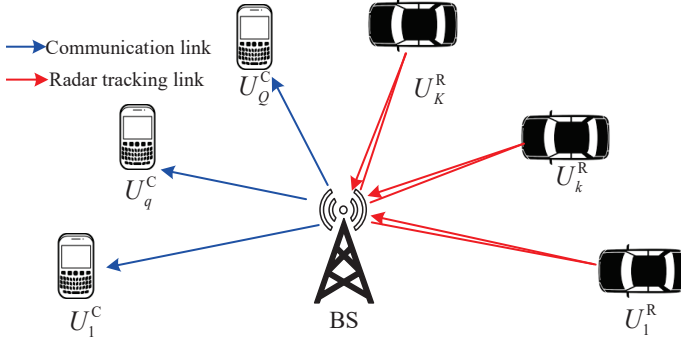


Fig. 1: A downlink DFRC system with one full-duplex BS, K tracking targets, and Q communication receivers.

a vector or a column vector of the main diagonal elements of a matrix. Finally, the circularly symmetric complex Gaussian (CSCG) distribution with mean μ and variance σ^2 is denoted as $\mathcal{CN}(\mu, \sigma^2)$.

II. SYSTEM MODEL

As shown in Fig. 1, we consider a downlink DFRC system, which is composed of one full-duplex BS equipped with L_t transmit antennas and L_r receive antennas, K radar tracking targets, denoted by U_k^R for $1 \leq k \leq K$, and Q single-antenna communication receivers, denoted by U_q^C for $1 \leq q \leq Q$. In order to reduce the training overhead and achieve high-efficient dual functions of mobility tracking for radar targets and information transmission for communication receivers, we need to first characterize the channel aging effects on the radar-communication performances with respect to the transmission time, and then propose the resource allocation scheme to dynamically optimize the channel re-estimation interval based on the system performance constraints. Hence, we propose the transmission frame structure consisting of multiple frames, as shown in Fig. 2. Specifically, each frame includes N transmission blocks and each block is with M symbol durations. In particular, the first block of each frame is divided into two phases, i.e., Phase-I for target tracking and channel estimation and Phase-II for information transmission. In Phase-I with M_1 symbol durations, the BS transmits training signals to track the mobility information of all targets. Simultaneously, the communication receivers utilize the received training signals to perform channel estimation and send feedback to the BS¹. In Phase-II with the remaining $(M - M_1)$ symbol durations, the BS transmits independent information to communication receivers by utilizing beamforming technology with the estimated CSI in Phase-I.

Moreover, we assume that the radar and communication channels are time-correlated among all transmission blocks in

¹Note that there will exist delay and quantification errors during the feedback processing. Low-resolution quantized CSI increases channel estimation error while higher-resolution quantized CSI increases feedback overhead. Both of them will degrade the transmission performance. Therefore, there is a performance trade-off between the quantification error and CSI feedback overhead. Considering the limited pages and system design complexity, we assume that the feedback delay and quantification error can be ignored and leave the relevant exploration of the influences of these factors as future extension works.

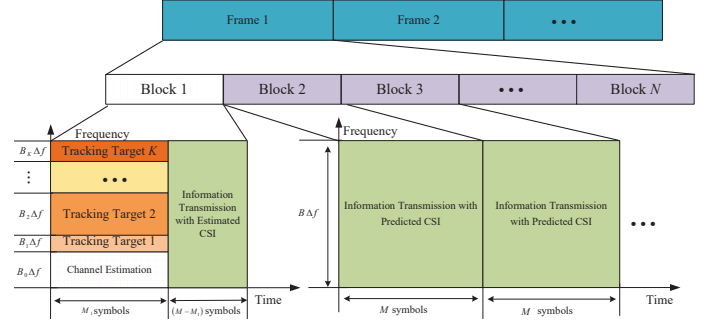


Fig. 2: Transmission frame structure, where each frame includes N blocks and each block is with M symbol durations.

each frame. Thus, in the remaining $(N - 1)$ blocks, the BS can predict the mobility information of all targets and the CSI of all communication users using the information estimated in the first block. By adopting this approach, the repeated transmission of dedicated signals for channel estimation and target tracking in the remaining blocks is eliminated, which can lower the training overhead and free up all radio resources for information transmission².

However, due to channel aging effects, the accuracies of the predicted mobility information and communication CSI may not support system performance requirements when the time increases. Therefore, we need to characterize the channel aging effects on the radar and communication performances, and then design the resource allocation scheme to improve the re-estimation interval N for overhead reduction and performance improvement subject to the specific sensing and communication demands for resource utilization efficiency improvement.

A. Signal Model

In this part, we introduce the signal models for radar target tracking and communication channel estimation in Phase-I of the first block, and information transmission in Phase-II of the first block and the remaining blocks.

As shown in Fig. 2, in Phase-I of the first block, the transmitted training signals for channel estimation and radar target tracking from the BS can be given by

$$\mathbf{s}(t) = \underbrace{\sqrt{p_0} \mathbf{w}_0(t) s_0(t)}_{\text{Channel estimation}} + \underbrace{\sum_{k=1}^K \sqrt{p_k} \mathbf{w}_k(t) s_k(t)}_{\text{Target tracking}}, \quad 0 \leq t \leq M_1 T, \quad (1)$$

where p_k and $\mathbf{w}_k(t) \in \mathbb{C}^{L_t \times 1}$ denote the downlink transmit power and beamformer with normalized power on the k -th

²Although communication signals in the remaining $(N - 1)$ blocks can be applied to target tracking, as shown in [15], we need to carefully design the downlink beamforming matrix to guarantee transmission and tracking performance. This is because the deployed large-scale antennas at the BS and separated target/receiver locations make the communication and radar channels nearly independent and orthogonal. Hence, it will not only decrease the communication performance but also increase the design complexity, thus making the performance analysis of the channel aging time effect very challenging. Besides, this paper focuses on channel aging time performance analysis instead of beamforming design, thus we only use the communication signal for data transmission in this paper.

band at time instant t , respectively. Here, $s_k(t)$ is the orthogonal frequency-division multiplexing (OFDM) modulated training signal on the k -th frequency band with B_k subcarriers, which is used to estimate the channels of all communication users if $k = 0$ or track the k -th target if $1 \leq k \leq K$, i.e.,

$$s_k(t) = \sum_{m=0}^{M_1-1} \sum_{b=0}^{B_k-1} \tilde{s}_{m,b}^k e^{j2\pi \left(\sum_{i=0}^{k-1} B_i + b \right) \Delta_f (t - T_{cp} - mT)} \times \text{rect}(t - mT), 0 \leq t \leq M_1 T, \quad (2)$$

where $\tilde{s}_{m,b}^k$ is the complex modulation symbol with power $\frac{1}{B_k}$ transmitted on the k -th band b -th subcarrier of the m -th OFDM symbol, T_{cp} is the duration of cyclic prefix, $T_o = \frac{1}{\Delta_f}$ is the OFDM elementary symbol duration, and $T = T_o + T_{cp}$ is the OFDM symbol duration including the cyclic prefix. Here, $B = \sum_{k=0}^K B_k$ and Δ_f are the total number of subcarriers and bandwidth of each subcarrier, respectively. The rectangular function is defined as $\text{rect}(x) = 1$ if $0 \leq x \leq T$, otherwise $\text{rect}(x) = 0$.

Next, in Phase-II of the first block and the remaining $(N - 1)$ blocks, let $c_{q,n}(t) \sim \mathcal{CN}(0, 1)$ be the data symbol transmitted to receiver U_q^C at time instant t during the n -th block. Then, the transmitted information signals to all communication receivers can be expressed as

$$\mathbf{s}(t) = \sum_{q=1}^Q \sqrt{\tilde{p}_{q,n}} \mathbf{f}_{q,n} c_{q,n}(t), \quad t \in \begin{cases} [M_1 T, n\tilde{T}], & \text{if } n = 1, \\ [(n-1)\tilde{T}, n\tilde{T}], & \text{if } 2 \leq n \leq N, \end{cases} \quad (3)$$

where $\tilde{T} = MT$. Here, $\tilde{p}_{q,n}$ and $\mathbf{f}_{q,n}(t) \in \mathbb{C}^{L_t \times 1}$ are the downlink transmit power and beamforming vector with normalized power, respectively, for receiver U_q^C at time instant t during the n -th block.

B. Radar and Communication Channel Aging Models

In this part, we introduce the radar and communication channel aging models, which are the basics to predict the target mobility information and communication CSI.

1) *Radar Channel Aging Model*: In the n -th transmission block, we regard the mobility information of target U_k^R as the information of its azimuth angle $\theta_{k,n}$, distance $d_{k,n}$, and velocity $v_{k,n}$ relative to the BS³, which is expressed by $\mathbf{x}_{k,n} = [\theta_{k,n}, d_{k,n}, v_{k,n}]^T \in \mathbb{C}^{3 \times 1}$. Based on the geometric relations between two successive blocks, as shown in Fig. 3, the target mobility state evolution model can be expressed as [27], [28]

$$\begin{cases} d_{k,n}^2 = d_{k,n-1}^2 + \Delta_{d_{k,n-1}}^2 - 2d_{k,n-1} \Delta_{d_{k,n-1}} \cos(\tilde{\theta}_{k,n-1}), \\ \frac{\Delta_{d_{k,n-1}}}{\sin(\theta_{k,n} - \theta_{k,n-1})} = \frac{d_{k,n}}{\sin(\tilde{\theta}_{k,n-1})}, \end{cases} \quad (4)$$

where $\Delta_{d_{k,n-1}} = v_{k,n-1} \tilde{T}$ and $\tilde{\theta}_{k,n-1} = \theta_{k,n-1} - \varphi_k$. Here, φ_k is the direction of velocity of U_k^R with respect to the

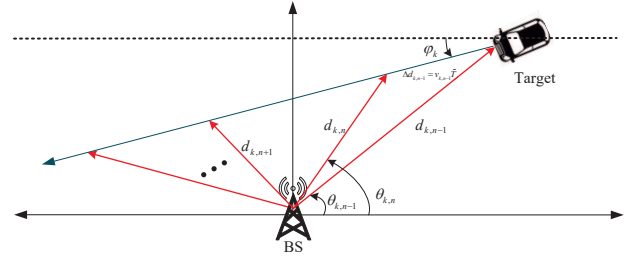


Fig. 3: Target mobility state evolution model.

negative horizontal direction of the BS. We assume that it is known at the BS and keeps constant in each block.

By using the similar approximation method in [27], the state evolution model in (4) can be approximated by

$$\begin{cases} \theta_{k,n} = \theta_{k,n-1} + d_{k,n-1}^{-1} v_{k,n-1} \tilde{T} \sin(\tilde{\theta}_{k,n-1}) + u_{k,n}^\theta, \\ d_{k,n} = d_{k,n-1} - v_{k,n-1} \tilde{T} \cos(\tilde{\theta}_{k,n-1}) + u_{k,n}^d, \\ v_{k,n} = v_{k,n-1} + u_{k,n}^v, \end{cases} \quad (5)$$

where $u_{k,n}^\theta$, $u_{k,n}^d$, and $u_{k,n}^v$ are the corresponding evaluation noises on the angle, distance, and velocity, respectively. Here, $u_{k,n}^\theta$, $u_{k,n}^d$, and $u_{k,n}^v$ are assumed to follow Gaussian distributions with means zero and variances δ_k^θ , δ_k^d , and δ_k^v , respectively.

From the approximated evaluation model in (5), the radar channel aging model within one-block time aging can be rewritten as

$$\mathbf{x}_{k,n} = \mathcal{G}(\mathbf{x}_{k,n-1}) + \mathbf{u}_{k,n}, \quad (6)$$

where $\mathcal{G}(\cdot)$ is the function dependent on (5), and $\mathbf{u}_{k,n} = [u_{k,n}^\theta, u_{k,n}^d, u_{k,n}^v]^T \in \mathbb{C}^{3 \times 1}$ is the noise with variance $\Sigma_k = \text{diag}(\delta_k^\theta, \delta_k^d, \delta_k^v) \in \mathbb{C}^{3 \times 3}$.

2) *Communication Channel Aging Model*: Here, we assume that there is no frequency selectivity on the communication channels for simplicity [37]⁴. Let $\mathbf{h}_{q,n} \in \mathbb{C}^{L_t \times 1}$ denote the downlink channel response from the BS to receiver U_q^C at the n -th block, which is assumed to follow Rayleigh fading, i.e., $\mathbf{h}_{q,0} \sim \mathcal{CN}(0, \beta_q \mathbf{I}_{L_t})$, where β_q denotes the large-scale fading effect. Then, the communication channel aging model within one-block time aging can be given by [31], i.e.,

$$\mathbf{h}_{q,n} = \rho_q \mathbf{h}_{q,n-1} + \sqrt{1 - \rho_q^2} \mathbf{e}_{q,n}, \quad (7)$$

where $\mathbf{e}_{q,n}$ is the uncorrelated complex Gaussian noise at the n -th block with assuming $\mathbf{e}_{q,n} \sim \mathcal{CN}(0, \beta_q \mathbf{I}_{L_t})$, and parameter ρ_q is the temporal correlation coefficient dependent on the doppler shift f_q of receiver U_q^C , which in Jakes' model is usually given by $\rho_q = J_0(2\pi f_q \tilde{T})$ and $J_0(\cdot)$ is the zeroth-order Bessel function of the first kind. Here, we assume that the velocity of each user keeps constant and the communication channel evolution is stationary. Thus, it can be off-line estimated by using the velocity estimator in [38]. Hence, ρ_q can be assumed to be known as prior information at the BS [35].

³Here, we assume that the uniform linear array is deployed at the BS, and we concentrate solely on the azimuth angle of the radar target, disregarding the elevation angle. As for the three-dimensional mobility tracking, it requires the deployment of the uniform planar array, which can be explored in a future extension due to page constraints.

⁴For the frequency selective communication channels, we can modify the transmission frame structure during Phase-II to estimate the CSI on other subcarriers. Besides, as for exploring the effect of channel aging time on frequency-selective channels, we leave it as an interesting topic for future research.

III. COMMUNICATION-RADAR PERFORMANCE ANALYSIS WITH CHANNEL AGING

In this section, we first analyze the radar tracking and channel estimation performances in the first block and then utilize the analyzed results to evaluate the tracking and communication performances within n -block time aging.

A. Radar Performance with Channel Aging

In this part, we first estimate the radar target mobility information and derive the corresponding CRLBs of estimated parameters in the first block. Then, we use the estimated results to evaluate the aged CRLBs in the n -th block without transmitting any training signals.

1) *Radar Channel Parameter Estimation:* In Phase-I of the first block, by transmitting the training signals defined in (1), the received reflected echoes at the BS on the k -th band through the round-trip radar channels are denoted by $\mathbf{y}_k^R(t) \in \mathbb{C}^{L_r \times 1}$ [37], i.e.,

$$\mathbf{y}_k^R(t) = \sum_{k'=1}^K [\sqrt{p_k L_r L_t} \alpha_{k',1} e^{j\phi_{k'}} \mathbf{a}(\theta_{k',1}) \mathbf{b}^H(\theta_{k',1}) \times \mathbf{w}_k(t) e^{j2\pi\nu_{k',1}^D t} s_k(t - \tau_{k',1})] + \omega_k^R(t), \quad (8)$$

where the upper subscript ‘‘R’’ implies the terms are related to the radar module and $\omega_k^R(t)$ is the received complex Gaussian noise at the BS with power spectral density σ . Here, $\alpha_{k,1} = \sqrt{\frac{c_0^2 \sigma_{\text{RCS},k}}{(4\pi)^3 f_c^2 d_{k,1}^4}}$, $\tau_{k,1} = \frac{2d_{k,1}}{c_0}$, and $\nu_{k,1}^D = \frac{2v_{k,1} \cos(\theta_{k,1} - \varphi_k)}{c_0} f_c$ are the attenuation factor due to the propagation through the overall round-trip path [39], [40], time delay, and doppler phase shift, respectively, corresponding to target U_k^R at the 1-th block. Besides, $\sigma_{\text{RCS},k}$ and ϕ_k are the complex radar cross-section (RCS) coefficient and additional random phase noise of target U_k^R , respectively. Finally, c_0 and f_c are the speed of light and subcarrier frequency, respectively, and $\mathbf{a}(\theta)$ and $\mathbf{b}(\theta)$ are the angle-of-arrival (AoA) and angle-of-departure (AoD) steering vectors with respect to angle θ , respectively. By setting the half-wavelength antenna spacing [41], we have $\mathbf{a}(\theta) = \frac{1}{\sqrt{L_r}} [1, e^{j\pi \sin \theta}, \dots, e^{j\pi(L_r-1) \sin \theta}]^H \in \mathbb{C}^{L_r \times 1}$ and $\mathbf{b}(\theta) = \frac{1}{\sqrt{L_t}} [1, e^{j\pi \sin \theta}, \dots, e^{j\pi(L_t-1) \sin \theta}]^H \in \mathbb{C}^{L_t \times 1}$.

Let $\mathbf{w}_k(t) = \mathbf{b}(\hat{\theta}_{k,1}^P)$ for $1 \leq k \leq K$, where $\hat{\theta}_{k,1}^P$ is the predicted angle based on the initial radar target mobility state $\mathbf{x}_{k,0}$ using (6). Note that the initial state $\mathbf{x}_{k,0}$ is assumed to be known at the BS, which can be regarded as the aged mobility information in the last frame. Then, (8) can be equivalently rewritten as

$$\hat{\mathbf{y}}_k^R(t) = \alpha_{k,1} e^{j\phi_k} \mathbf{a}(\theta_{k,1}) e^{j2\pi\nu_{k,1}^D t} s_k(t - \tau_{k,1}) + \hat{\omega}_k^R(t), \quad (9)$$

where $\hat{\omega}_k^R(t) = \frac{(\omega_k^R(t) + \boldsymbol{\eta}_k(t))}{\sqrt{p_k L_r L_t \chi_{k,k}}}$ is the interference-plus-noise term with $\chi_{k,i} = \mathbf{b}^H(\theta_{i,1}) \mathbf{b}(\hat{\theta}_{k,1}^P)$. Here, $\boldsymbol{\eta}_k(t) = \sum_{k' \neq k}^K \sqrt{p_k} \alpha_{k',1} e^{j\phi_{k'}} \mathbf{a}(\theta_{k',1}) \chi_{k',k} e^{j2\pi\nu_{k',1}^D t} s_k(t - \tau_{k',1})$ is the interference caused by the reflected echoes of $s_k(t)$ from target $U_{k'}^R$.

By sampling $\hat{\mathbf{y}}_k^R(t)$ in (9) at each $t = mT + T_{cp} + \frac{b}{B_k} T_o$ after bandpass filtering and down conversion, we have

$$\tilde{\mathbf{y}}_k^R(m, b) \approx \alpha_{k,1} e^{j\phi_k} \mathbf{a}(\theta_{k,1}) e^{j2\pi m T \nu_{k,1}^D} \times \sum_{i=0}^{B_k-1} \tilde{s}_{m,i}^k e^{j2\pi \frac{ib}{B_k}} e^{-j2\pi i \Delta_f \tau_{k,1}} + \hat{\omega}_k^R(m, b), \quad (10)$$

with assuming $\nu_{k,1}^D \ll \Delta_f$, where $\hat{\omega}_k^R(m, b)$ is the sampled $\hat{\omega}_k^R(t)$. After applying the discrete Fourier transform (DFT), we have

$$\bar{\mathbf{y}}_k^R(m, b) = \frac{1}{\tilde{s}_{m,b}^k B_k} \sum_{i'=0}^{B_k-1} \tilde{\mathbf{y}}_k^R(m, i') e^{-j2\pi \frac{i'b}{B_k}} \approx \alpha_{k,1} e^{j\phi_k} \mathbf{a}(\theta_{k,1}) e^{j2\pi m T \nu_{k,1}^D} e^{-j2\pi b \Delta_f \tau_{k,1}} + \bar{\omega}_k^R(m, b), \quad (11)$$

where $\bar{\omega}_k^R(m, b)$ is the corresponding noise.

From (11), the angle of U_k^R in the first block can be estimated by

$$\hat{\theta}_{k,1} = \arg \max_{\theta} \sum_{m=0}^{M_1-1} \sum_{b=0}^{B_k-1} |\mathbf{a}^H(\theta) \bar{\mathbf{y}}_k^R(m, b)|^2. \quad (12)$$

Then, with the estimated angle $\hat{\theta}_{k,1}$, we apply the Periodogram-based method [42] to estimate the distance and velocity of U_k^R . Specifically, we define $\mathcal{Y}_k(\tau, \nu^D)$ as

$$\mathcal{Y}_k(\tau, \nu^D) = \sum_{m=0}^{M_1-1} \sum_{b=0}^{B_k-1} \mathbf{a}^H(\hat{\theta}_{k,1}) \bar{\mathbf{y}}_k^R(m, b) e^{-j2\pi m T \nu^D} e^{j2\pi b \Delta_f \tau}. \quad (13)$$

Then, the time delay and doppler phase shift can be estimated by

$$(\hat{\tau}_{k,1}, \hat{\nu}_{k,1}^D) = \arg \max_{\tau, \nu^D} |\mathcal{Y}_k(\tau, \nu^D)|^2. \quad (14)$$

Finally, the distance and velocity of U_k^R in the first block can be estimated by

$$\hat{d}_{k,1} = \frac{1}{2} \hat{\tau}_{k,1} c_0, \quad (15)$$

$$\hat{v}_{k,1} = \frac{\hat{\nu}_{k,1}^D c_0}{2f_c \cos(\hat{\theta}_{k,1} - \varphi_k)}. \quad (16)$$

2) *Radar Tracking Performances in Block 1:* Here, we derive the CRLBs from the received signal model in (11) for radar tracking performance analysis.

To begin with, by applying some algebraic manipulations of $\chi_{k,i}$ in (9), we have $|\chi_{k,i}| = \frac{|\sin(\frac{L_t \pi}{2} \Delta_{k,i}^\theta)|}{L_t |\sin(\frac{\pi}{2} \Delta_{k,i}^\theta)|}$, where $\Delta_{k,i}^\theta = \sin(\theta_{i,1}) - \sin(\hat{\theta}_{k,1}^P)$. Then, we have $|\chi_{k,i}| = 1$ if $\Delta_{k,i}^\theta = 0$ and $|\chi_{k,i}| = 0$ if $-2 < \Delta_{k,i}^\theta < 2$ for large scale transmit antenna array, i.e., $L_t \rightarrow \infty$. Next, in order to analyze the distribution of $\bar{\omega}_k^R(m, b)$ in (11), we apply the approximation that $|\chi_{k,k}| = 1$ for $1 \leq k \leq K$ and $\chi_{k,i} = 0$ for $1 \leq k \neq i \leq K$ by ignoring the bias of the predicted angle. Note that we only apply this approximation in performance analysis, and the non-zero bias exists in $\Delta_{k,k}^\theta$ and $|\chi_{k,k}|$ may be smaller than one in practice/simulations. Nevertheless, this approximation only affects the noise power analysis but does

no changes to the procedure of the proposed analysis method. From simulation results in Fig. 4, we observe that the non-zero bias does not influence the analyzed performance results much. Then, the noise $\bar{\omega}_k^R(m, b)$ in (11) is approximated by

$$\bar{\omega}_k^R(m, b) \approx \frac{\sum_{i'=0}^{B_k-1} \omega_k^R(m, b) e^{-j2\pi \frac{i'b}{B_k}}}{\tilde{s}_{m,b}^k B_k \sqrt{p_k L_r L_t}}, \quad (17)$$

where $\omega_k^R(m, b)$ is the sampled $\omega_k^R(t)$. Hence, we can know $\bar{\omega}_k^R(m, b)$ can be approximated as Gaussian distribution with mean zero and variance $\frac{\sigma_{\Delta_f}}{p_k L_r L_t} \mathbf{I}_{L_r}$.

Next, the CRLBs of radar target tracking in block 1 are given in the following theorem⁵.

Theorem 3.1: In the regime of large L_t , the CRLBs on the estimation MSEs of $\theta_{k,1}$, distance $d_{k,1}$, and velocity $v_{k,1}$ for U_k^R in block 1 can be approximated by

$$\mathbb{E} \left(\left\| \theta_{k,1} - \hat{\theta}_{k,1} \right\|^2 \right) \geq \frac{\sigma_k^\theta}{p_k B_k M_1}, \quad (18a)$$

$$\mathbb{E} \left(\left\| d_{k,1} - \hat{d}_{k,1} \right\|^2 \right) \geq \frac{\sigma_k^d}{p_k B_k M_1 (B_k^2 - 1)}, \quad (18b)$$

$$\mathbb{E} \left(\left\| v_{k,1} - \hat{v}_{k,1} \right\|^2 \right) \geq \frac{\sigma_k^v}{p_k B_k M_1 (M_1^2 - 1)}, \quad (18c)$$

where $\sigma_k^\theta = \frac{6\sigma_{\Delta_f}}{|\alpha_{k,1}|^2 \pi^2 \cos^2(\theta_{k,1}) L_t L_r (L_r^2 - 1)}$, $\sigma_k^d = \frac{3c_0^2 \sigma_{\Delta_f}}{8(\pi \Delta_f)^2 |\alpha_{k,1}|^2 L_t L_r}$, and $\sigma_k^v = \frac{3c_0^2 \sigma_{\Delta_f}}{8(\pi T)^2 f_c^2 |\alpha_{k,1}|^2 \cos^2(\theta_{k,1}) L_t L_r}$.

Proof: Please refer to Appendix A. ■

3) *Aged Radar Tracking Performances in Block n:* In the following, we define the estimation/prediction error covariance matrix in the n -th block as

$$\mathbf{E}_{k,n} = \mathbb{E} \left((\mathbf{x}_{k,n} - \hat{\mathbf{x}}_{k,n}) (\mathbf{x}_{k,n} - \hat{\mathbf{x}}_{k,n})^H \right) \in \mathbb{C}^{3 \times 3}, \quad (19)$$

where $\hat{\mathbf{x}}_{k,n}$ is the aged radar mobility information in the n -th block.

From (6), the aged information $\hat{\mathbf{x}}_{k,n}$ can be predicted if $\hat{\mathbf{x}}_{k,n-1}$ is already known, i.e.,

$$\hat{\mathbf{x}}_{k,n} = \mathcal{G}(\hat{\mathbf{x}}_{k,n-1}). \quad (20)$$

However, since $\mathcal{G}(\cdot)$ defined in (6) is a nonlinear function, it is difficult to derive the aged tracking performance analytically. Thus, we apply the linear approximation for $\mathcal{G}(\cdot)$ in (6), i.e.,

$$\mathbf{x}_{k,n} \approx \mathcal{G}(\hat{\mathbf{x}}_{k,n-1}) + \mathbf{G}_{k,n-1} (\mathbf{x}_{k,n-1} - \hat{\mathbf{x}}_{k,n-1}) + \mathbf{u}_{k,n}, \quad (21)$$

where $\mathbf{G}_{k,n-1} \in \mathbb{C}^{3 \times 3}$ is the Jacobian matrix for $\partial \mathcal{G}(\mathbf{x}_{k,n-1})$, i.e., $\mathbf{G}_{k,n-1} = \left. \frac{\partial \mathcal{G}(\mathbf{x}_k)}{\partial \mathbf{x}_k} \right|_{\mathbf{x}_k = \hat{\mathbf{x}}_{k,n-1}}$.

Next, by substituting (20) and (21) into (19), matrix $\mathbf{E}_{k,n}$ can be rewritten as

$$\begin{aligned} \mathbf{E}_{k,n} &= \mathbb{E} \left((\mathbf{x}_{k,n} - \mathcal{G}(\hat{\mathbf{x}}_{k,n-1})) (\mathbf{x}_{k,n} - \mathcal{G}(\hat{\mathbf{x}}_{k,n-1}))^H \right) \\ &= \mathbf{G}_{k,n-1} \mathbf{E}_{k,n-1} \mathbf{G}_{k,n-1}^H + \Sigma_k, \end{aligned} \quad (22)$$

⁵Note that applying other compressive algorithms may improve the estimation accuracy, but the derived results are the lower bounds of any unbiased estimators [43], which depend on the statics information in (11) instead of estimation algorithms. Hence, we do not provide other estimation algorithms due to the limited pages.

where Σ_k is defined in (6). After some algebraic manipulations, $\mathbf{E}_{k,n}$ for $2 \leq n \leq N$ can be rewritten as a function of $\mathbf{E}_{k,1}$, i.e.,

$$\mathbf{E}_{k,n} = \tilde{\mathbf{G}}_{k,n-1} \mathbf{E}_{k,1} \tilde{\mathbf{G}}_{k,n-1}^H + \sum_{i=1}^{n-1} \tilde{\mathbf{G}}_{k,n,i} \Sigma_k \tilde{\mathbf{G}}_{k,n,i}^H, \quad (23)$$

where $\tilde{\mathbf{G}}_{k,n-1} \in \mathbb{C}^{3 \times 3}$ and $\tilde{\mathbf{G}}_{k,n,i} \in \mathbb{C}^{3 \times 3}$ are given by

$$\tilde{\mathbf{G}}_{k,n-1} = \prod_{i=1}^{n-1} \mathbf{G}_{k,i} \quad \text{and} \quad \tilde{\mathbf{G}}_{k,n,i} = \begin{cases} \mathbf{I}_3, & i=1, \\ \prod_{i'=i}^{n-1} \mathbf{G}_{k,i'}, & i \geq 2, \end{cases} \quad (24)$$

respectively. By using the CRLBs obtained in (18), we have

$$\begin{aligned} \mathbf{E}_{k,1} &\succeq \text{diag} \left(\frac{\sigma_k^\theta}{p_k B_k M_1}, \frac{\sigma_k^d}{p_k B_k M_1 (B_k^2 - 1)}, \frac{\sigma_k^v}{p_k B_k M_1 (M_1^2 - 1)} \right) \\ &\triangleq \mathbf{D}_k. \end{aligned} \quad (25)$$

By substituting (25) into (23), we have

$$\begin{aligned} \mathbf{E}_{k,n} &\succeq \tilde{\mathbf{G}}_{k,n-1} \mathbf{D}_k \tilde{\mathbf{G}}_{k,n-1}^H + \sum_{i=1}^{n-1} \tilde{\mathbf{G}}_{k,n,i} \Sigma_k \tilde{\mathbf{G}}_{k,n,i}^H \\ &\triangleq \tilde{\mathbf{E}}_{k,n}. \end{aligned} \quad (26)$$

Thus, the aged CRLBs on the predicted MSEs of $\theta_{k,n}$, distance $d_{k,n}$, and velocity $v_{k,n}$ for U_k^R in block n are given by

$$\mathbb{E} \left(\left\| \theta_{k,n} - \hat{\theta}_{k,n} \right\|^2 \right) \geq \tilde{\mathbf{E}}_{k,n}(1, 1) \triangleq \mathcal{C}(\hat{\theta}_{k,n}), \quad (27a)$$

$$\mathbb{E} \left(\left\| d_{k,n} - \hat{d}_{k,n} \right\|^2 \right) \geq \tilde{\mathbf{E}}_{k,n}(2, 2) \triangleq \mathcal{C}(\hat{d}_{k,n}), \quad (27b)$$

$$\mathbb{E} \left(\left\| v_{k,n} - \hat{v}_{k,n} \right\|^2 \right) \geq \tilde{\mathbf{E}}_{k,n}(3, 3) \triangleq \mathcal{C}(\hat{v}_{k,n}). \quad (27c)$$

However, considering the matrix multiplication of polynomials in $\tilde{\mathbf{G}}_{k,n-1}$ and $\tilde{\mathbf{G}}_{k,n,i}$, it is still hard to apply the aged radar tracking performance in (27) to study the resource allocation scheme design. Therefore, we propose the following theorem to further approximate the CRLBs in (27), thus obtaining the simplified expressions.

Theorem 3.2: The aged CRLBs on the predicted MSEs of $\theta_{k,n}$, distance $d_{k,n}$, and velocity $v_{k,n}$ for U_k^R in block n derived in (27) can be approximated by

$$\begin{aligned} \mathcal{C}(\hat{\theta}_{k,n}) &\approx \frac{a_{k,n} \sigma_k^\theta}{p_k B_k M_1} + b_{k,n} \delta_k^\theta \\ &\triangleq \tilde{\mathcal{C}}(\hat{\theta}_{k,n}), \end{aligned} \quad (28a)$$

$$\begin{aligned} \mathcal{C}(\hat{d}_{k,n}) &\approx \frac{\sigma_k^d}{p_k B_k M_1 (B_k^2 - 1)} + (n-1) \delta_k^d \\ &\triangleq \tilde{\mathcal{C}}(\hat{d}_{k,n}), \end{aligned} \quad (28b)$$

$$\begin{aligned} \mathcal{C}(\hat{v}_{k,n}) &\approx \frac{\sigma_k^v}{p_k B_k M_1 (M_1^2 - 1)} + (n-1) \delta_k^v \\ &\triangleq \tilde{\mathcal{C}}(\hat{v}_{k,n}), \end{aligned} \quad (28c)$$

where $a_{k,n} = \left| 1 + \sum_{i=1}^{n-1} \frac{\hat{v}_{k,i} \tilde{T}}{\hat{d}_{k,i}} \cos(\hat{\theta}_{k,i}) \right|^2$, $b_{k,n} = 1 + \sum_{i=2}^{n-1} \left| 1 + \sum_{i'=i}^{n-1} \frac{\hat{v}_{k,i'} \tilde{T}}{\hat{d}_{k,i'}} \cos(\hat{\theta}_{k,i'}) \right|^2$, and $\hat{\theta}_{k,n} = \hat{\theta}_{k,n} - \varphi_k$.

Proof: Please refer to Appendix B. ■

Note that from the simulation results in Fig. 4, we know that the proposed approximated CRLBs in (28) can achieve nearly identical performances to that in (27).

B. Communication Performance with Channel Aging

In this part, we first estimate the CSI of all communication receivers in the first block and use them to predict the CSI in the n -th block. Then, we analyze the channel estimation/prediction error and derive the total aged achievable rate of all receivers.

1) *Communication CSI Estimation and Prediction:* In Phase-I of the first transmission block, by transmitting the training signals in (1), the received signals at U_q^C are given by

$$y_{q,1}^C(t) = \mathbf{h}_{q,1}^H \mathbf{w}_0(t) \sum_{m=0}^{M_1-1} \sum_{b=0}^{B_0-1} \tilde{s}_{m,b}^0 e^{j2\pi b \Delta_f (t - T_{cp} - mT)} \times \text{rect}(t - mT) + \omega_{q,1}^C(t), \quad (29)$$

where the upper subscript ‘‘C’’ implies the terms are related to the communication module. The term $\omega_{q,1}^C(t)$ is the received Gaussian noise with power spectral density σ_q^C .

Similar as the processes in (10) and (11), by sampling $y_{q,1}^C(t)$ in (29) at each $t = mT + T_{cp} + \frac{b}{B_k} T_o$ after bandpass filtering, and setting the corresponding transmit beamformer $\mathbf{w}_0(t)$ as $\mathbf{f}_0(m)$, we can apply the DFT for the sampled signals and have

$$\begin{aligned} \bar{y}_{q,1}^C(m, b) &= \frac{1}{\tilde{s}_{m,b}^0 B_0} \sum_{i'=0}^{B_0-1} \tilde{y}_q^C(m, i') e^{-j2\pi \frac{i'b}{B_0}} \\ &\approx \sqrt{p_0} \mathbf{h}_{q,1}^H \mathbf{f}_0(m) + \bar{\omega}_{q,1}^C(m, b), \end{aligned} \quad (30)$$

where $\bar{\omega}_{q,1}^C(m, b)$ is the approximated Gaussian noise with mean zero and variance $\tilde{\sigma}_q = \sigma_q^C \Delta_f$. Then, during the m -th OFDM symbol duration, we have

$$\begin{aligned} \bar{\mathbf{y}}_{q,1}^C(m) &= \frac{1}{B_0} \sum_{b=1}^{B_0} \bar{y}_{q,1}^C(m, b) \\ &\approx \sqrt{p_0} \mathbf{h}_{q,1}^H \mathbf{f}_0(m) + \bar{\omega}_{q,1}^C(m), \end{aligned} \quad (31)$$

where $\bar{\omega}_{q,1}^C(m)$ is the equivalent Gaussian noise with mean zero and variance $\frac{\tilde{\sigma}_q}{B_0}$.

Then, denoting $\bar{\mathbf{y}}_{q,1}^C = [\bar{y}_{q,1}^C(0), \dots, \bar{y}_{q,1}^C(M_1 - 1)]^H \in \mathbb{C}^{M_1 \times 1}$ and $\mathbf{F}_0 = [\mathbf{f}_0(0), \dots, \mathbf{f}_0(M_1 - 1)] \in \mathbb{C}^{L_t \times M_1}$, we can rewrite (31) as the following matrix form, i.e.,

$$\bar{\mathbf{y}}_{q,1}^C = \sqrt{p_0} \mathbf{F}_0^H \mathbf{h}_{q,1} + \bar{\omega}_{q,1}^C, \quad (32)$$

where $\bar{\omega}_{q,1}^C \in \mathbb{C}^{M_1 \times 1}$ is the received noise, i.e., $\bar{\omega}_{q,1}^C \sim \mathcal{CN}\left(0, \frac{\tilde{\sigma}_q}{B_0} \mathbf{I}_{M_1}\right)$.

By setting \mathbf{F}_0 satisfying $\mathbf{F}_0 \mathbf{F}_0^H = \frac{M_1}{L_t} \mathbf{I}_{L_t}$, the linear MMSE channel estimator is given by [34]

$$\hat{\mathbf{h}}_{q,1} = \left(1 + \frac{L_t \tilde{\sigma}_q}{M_1 B_0 p_0} \times \frac{1}{\beta_q}\right)^{-1} \left(\frac{1}{\sqrt{p_0}} \mathbf{F}_0^\dagger \bar{\mathbf{y}}_{q,1}^C\right), \quad (33)$$

where \mathbf{F}_0^\dagger is the Moore-Penrose pseudoinverse of matrix \mathbf{F}_0 .

From (33), it can be proved that $\hat{\mathbf{h}}_{q,1} \sim \mathcal{CN}(0, \lambda_q \mathbf{I}_{L_t})$ where $\lambda_q = \frac{M_1 \beta_q^2 p_0 B_0}{L_t \tilde{\sigma}_q + M_1 \beta_q p_0 B_0}$. By using the orthogonality property of MMSE, channel $\mathbf{h}_{q,1}$ can be represented by

$$\mathbf{h}_{q,1} = \hat{\mathbf{h}}_{q,1} + \tilde{\mathbf{h}}_{q,1}, \quad (34)$$

where $\tilde{\mathbf{h}}_{q,1} \sim \mathcal{CN}(0, (\beta_q - \lambda_q) \mathbf{I}_{L_t})$ is the corresponding channel estimation error.

By applying algebraic manipulations with the channel aging model in (7), $\mathbf{h}_{q,n}$ is rewritten by

$$\mathbf{h}_{q,n} = \rho_q^{n-1} \mathbf{h}_{q,1} + \sqrt{1 - \rho_q^{2(n-1)}} \tilde{\mathbf{e}}_{q,n}, \quad (35)$$

where $\tilde{\mathbf{e}}_{q,n} = \frac{1}{\sqrt{1 - \rho_q^{2(n-1)}}} \sum_{i=0}^{n-2} \rho_q^i \sqrt{1 - \rho_q^2} \mathbf{e}_{q,n-i}$ is called aging noise, which follows complex Gaussian distribution, i.e., $\tilde{\mathbf{e}}_{q,n} \sim \mathcal{CN}(0, \beta_q \mathbf{I}_{L_t})$.

Then, by substituting (34) into (35), we have

$$\mathbf{h}_{q,n} = \rho_q^{n-1} \hat{\mathbf{h}}_{q,1} + \rho_q^{n-1} \tilde{\mathbf{h}}_{q,1} + \sqrt{1 - \rho_q^{2(n-1)}} \tilde{\mathbf{e}}_{q,n}. \quad (36)$$

The predicted CSI of receiver U_q^R in the n -th block can be given by [35]

$$\hat{\mathbf{h}}_{q,n} = \rho_q^{n-1} \hat{\mathbf{h}}_{q,1}, \quad (37)$$

whose prediction error is $\bar{\mathbf{e}}_{q,n} = \rho_q^{n-1} \tilde{\mathbf{h}}_{q,1} + \sqrt{1 - \rho_q^{2(n-1)}} \tilde{\mathbf{e}}_{q,n}$, which follows complex Gaussian distribution, i.e., $\bar{\mathbf{e}}_{q,n} \sim \mathcal{CN}(0, (\beta_q - \rho_q^{2n-2} \lambda_q) \mathbf{I}_{L_t})$.

2) *Total Aged Achievable Rate:* Based on the data signals defined in (3), the received signals at U_q^C in the n -th block can be rewritten as

$$\begin{aligned} y_{q,n}^C(t) &= \mathbf{h}_{q,n}^H \sum_{i=1}^Q \sqrt{\tilde{p}_{i,n}} \mathbf{f}_{i,n} c_{i,n}(t) + \omega_{q,n}^C(t) \\ &= \sqrt{\tilde{p}_{q,n}} \mathbb{E}(\mathbf{h}_{q,n}^H \mathbf{f}_{q,n}) c_{q,n}(t) + \zeta_{q,n}(t) + \tilde{\zeta}_{q,n}(t) + \omega_{q,n}^C(t), \end{aligned} \quad (38)$$

where $\omega_{q,n}^C(t)$ is the received Gaussian noise with mean zero and variance $\tilde{\sigma}_q$, and interference terms $\zeta_{q,n}(t)$ and $\tilde{\zeta}_{q,n}(t)$ are given by

$$\zeta_{q,n}(t) = \sqrt{\tilde{p}_{q,n}} [\mathbf{h}_{q,n}^H \mathbf{f}_{q,n} - \mathbb{E}(\mathbf{h}_{q,n}^H \mathbf{f}_{q,n})] c_{q,n}(t), \quad (39)$$

$$\tilde{\zeta}_{q,n}(t) = \mathbf{h}_{q,n}^H \sum_{i \neq q}^Q \sqrt{\tilde{p}_{i,n}} \mathbf{f}_{i,n} c_{i,n}(t), \quad (40)$$

respectively. Then, the achievable rate (bits/s/Hz) of U_q^C in the n -th block is

$$R_{q,n} = \frac{M'_n}{M} \log_2(1 + \tilde{p}_{q,n} \gamma_{q,n}), \quad (41)$$

where $M'_1 = M - M_1$, $M'_n = M$ for $2 \leq n \leq N$, and

$$\gamma_{q,n} = \frac{|\mathbb{E}(\mathbf{h}_{q,n}^H \mathbf{f}_{q,n})|^2}{\mathbb{E}(|\zeta_{q,n}(t)|^2) + \mathbb{E}(|\tilde{\zeta}_{q,n}(t)|^2) + \tilde{\sigma}_q}. \quad (42)$$

Based on the predicted CSI in (37), the MRT and ZF transmit beamforming vectors for each U_q^C are given by

$$\mathbf{f}_{q,n} = \begin{cases} \frac{\hat{\mathbf{h}}_{q,1}}{\sqrt{\mathbb{E}(\|\hat{\mathbf{h}}_{q,1}\|^2)}} = \frac{1}{\sqrt{\lambda_q L_t}} \hat{\mathbf{h}}_{q,1}, \text{MRT}, \\ \frac{\mathbf{a}_q}{\sqrt{\mathbb{E}(\|\mathbf{a}_q\|^2)}} \stackrel{(a)}{=} \sqrt{\lambda_q (L_t - Q)} \mathbf{a}_q, \text{ZF}, \end{cases} \quad (43)$$

respectively, where \mathbf{a}_q is the q -th column of matrix $\hat{\mathbf{H}}_1 (\hat{\mathbf{H}}_1^H \hat{\mathbf{H}}_1)^{-1}$ with $\hat{\mathbf{H}}_1 = [\hat{\mathbf{h}}_{1,1}, \hat{\mathbf{h}}_{2,1}, \dots, \hat{\mathbf{h}}_{Q,1}] \in \mathbb{C}^{L_t \times Q}$ and (a) is due to $\mathbb{E}(\|\mathbf{a}_q\|^2) = \frac{1}{\lambda_q (L_t - Q)}$ for the scenario $L_t \geq (Q + 1)$ [44].

Theorem 3.3: In the n -th aged block, with the predicted CSI in (37), parameter $\gamma_{q,n}$ in (42) using MRT or ZF transmit beamforming is given by

$$\gamma_{q,n} = \begin{cases} \frac{\rho_q^{2(n-1)} M_1 \beta_q^2 p_0 B_0 L_t}{(P \beta_q + \bar{\sigma}_q)(L_t \bar{\sigma}_q + M_1 \beta_q p_0 B_0)}, \text{MRT}, \\ \frac{\rho_q^{2(n-1)} M_1 \beta_q^2 p_0 B_0 (L_t - Q)}{(P \beta_q + \bar{\sigma}_q)(L_t \bar{\sigma}_q + M_1 \beta_q p_0 B_0) - \rho_q^{2(n-1)} P M_1 \beta_q^2 p_0 B_0}, \text{ZF}. \end{cases} \quad (44)$$

Proof: Please refer to Appendix C. \blacksquare

Let the total achievable rate in the n -th block be $R_n = \sum_{q=1}^Q R_{q,n}$. Based on Theorem 3.3, it is straightforward to have the following asymptotic analysis of R_n with respect to the transmit power, i.e.,

$$\lim_{P \rightarrow \infty} R_n \rightarrow \begin{cases} \frac{M'_n}{M} \sum_{q=1}^Q \log_2 \left(1 + \rho_q^{2(n-1)} \kappa_{q,n} L_t \right), \text{MRT}, \\ \frac{M'_n}{M} \sum_{q=1}^Q \log_2 \left(1 + \frac{\rho_q^{2(n-1)}}{1 - \rho_q^{2(n-1)}} \kappa_{q,n} (L_t - Q) \right), \text{ZF}, \end{cases} \quad (45)$$

where $\kappa_{q,n} = \frac{\tilde{p}_{q,n}}{P}$. From (45), it can be observed that the achievable rates under MRT and ZF beamforming decrease as the channel aging time increases.

IV. AVERAGE TOTAL ACHIEVABLE RATE MAXIMIZATION WITH CHANNEL AGING

In this section, we use the characterized aged radar tracking and communication performance metrics to study the situation-dependent resource allocation scheme considering the individual target tracking precision demand and communication rate requirement. In particular, we first provide the problem formulation and then provide the suboptimal algorithm to solve it efficiently.

A. Problem Formulation

From (28) and (44), besides the channel aging time, we know bandwidth and power allocations are also key factors that affect the aged communication and radar tracking performance. Therefore, in this paper, we aim to jointly optimize the number of subcarriers $\mathbf{B} = [B_0, \dots, B_K]^T \in \mathbb{C}^{(K+1) \times 1}$ and transmit power $\mathbf{p} = [p_0, \dots, p_K]^T \in \mathbb{C}^{(K+1) \times 1}$ for channel training in Phase-I of the first block, transmit power $\tilde{\mathbf{p}} = [\tilde{p}_{1,1}, \dots, \tilde{p}_{q,n}, \dots, \tilde{p}_{Q,N}]^T \in \mathbb{C}^{Q \times 1}$ for data transmission in Phase-II of the first block and remaining blocks,

and channel re-estimation interval N , to maximize the average total achievable rate subject to various practical constraints. Mathematically, we have the following optimization problem:

$$\begin{aligned} \mathbf{P1} : \quad & \max_{N, \mathbf{p}, \tilde{\mathbf{p}}, \mathbf{B}} \mathcal{R}(N, \mathbf{p}, \tilde{\mathbf{p}}, \mathbf{B}) = \frac{1}{N} \sum_{n=1}^N \sum_{q=1}^Q R_{q,n} \\ & \text{s.t.} \quad \text{C1} : \tilde{\mathcal{C}}(\hat{\theta}_{k,n}) \leq \Gamma_{k,\max}^\theta, \forall n, 1 \leq k \leq K, \\ & \quad \text{C2} : \tilde{\mathcal{C}}(\hat{d}_{k,n}) \leq \Gamma_{k,\max}^d, \forall n, 1 \leq k \leq K, \\ & \quad \text{C3} : \tilde{\mathcal{C}}(\hat{v}_{k,n}) \leq \Gamma_{k,\max}^v, \forall n, 1 \leq k \leq K, \\ & \quad \text{C4} : R_{q,n} \geq R_{q,\min}, \forall q, n, \\ & \quad \text{C5} : \sum_{k=0}^K p_k \leq P, \\ & \quad \text{C6} : \sum_{q=1}^Q \tilde{p}_{q,n} \leq P, \forall n, \\ & \quad \text{C7} : \sum_{k=0}^K B_k \leq B, \\ & \quad \text{C8} : 0 \leq p_k, \forall k, \\ & \quad \text{C9} : 0 \leq \tilde{p}_{q,n}, \forall q, n, \\ & \quad \text{C10} : B_k \in \mathbb{N}, \forall k, \end{aligned}$$

where $\Gamma_{k,\max}^\theta$, $\Gamma_{k,\max}^d$, and $\Gamma_{k,\max}^v$ are tracking error constraints of target U_k^R with respect to its angle, distance, and velocity, respectively, while $R_{q,\min}$ is the minimum transmission rate required by receiver U_q^C . Specifically, C1, C2, and C3 are the individual radar tracking accuracy requirements and C4 is the individual communication data rate requirement. C5 and C6 are the total transmission power constraints in the training and data transmission stages, respectively. C7 is the total number of subcarriers constraint. Finally, C8, C9, and C10 are practical constraints.

B. Algorithm Development

To begin with, considering integer constraint C10, problem **P1** is MINLP in general. Thus, it is a non-convex optimization problem, and obtaining its optimal solution may introduce intractable computational complexity. In the following, we propose an efficient two-step based suboptimal algorithm to solve problem **P1**. Specifically, in the first step, we solve the relaxed continuous variable optimization problem of **P1** by replacing constraint C10 as $0 \leq B_k, \forall k$, i.e.,

$$\begin{aligned} \mathbf{P2} : \quad & \max_{N, \mathbf{p}, \tilde{\mathbf{p}}, \mathbf{B}} \mathcal{R}(N, \mathbf{p}, \tilde{\mathbf{p}}, \mathbf{B}) \\ & \text{s.t.} \quad 0 \leq B_k, \forall k, \\ & \quad \text{C1} - \text{C8}, \end{aligned} \quad (47)$$

Then, in the second step, we apply an integer conversion method to make the solutions of B_k satisfy C10. Note that the optimal solution of problem **P2** is the upper bound of the original problem **P1** because the relaxed constraints can introduce a large feasibility region.

However, **P2** is still non-convex due to the coupled optimization variables. Furthermore, the numbers of optimization variables and conditions vary with the channel aging time N , which increases the difficulties in solving this problem. Therefore, to find the optimal solution of **P2**, we propose a

one-dimensional search based optimization algorithm thanks to the channel aging time N belonging to one-dimensional variable. In this algorithm, we use a one-dimensional exhaustive search for all possible channel aging time N , and we propose algorithms to solve **P2** optimally for each fixed N . Then, we can obtain the optimal solution of **P2** with the optimal N that makes the objective maximum.

Next, in the following two theorems, we first analyze the potential upper bound of channel aging time N to reduce search region in the one-dimensional search for complexity reduction, and then provide the way to find the optimal solution of **P2** with a fixed N .

Theorem 4.1: If problem **P2** is feasible, the maximum potential feasible channel aging time N should be smaller than the following bound, i.e.,

$$N_{\max} = \min_{\forall k, \forall q} \{N_{k, \max}^R, N_{q, \max}^C\}, \quad (48)$$

where $N_{k, \max}^R$ and $N_{q, \max}^C$ are the potential maximum channel aging time N for target U_k^R and receiver U_q^C , respectively, which are given by

$$N_{k, \max}^R = 1 + \min \left\{ \left\lfloor \frac{\Gamma_{k, \max}^d}{\delta_k^d} - \frac{\sigma_k^d}{\delta_k^d P B M_1 (B^2 - 1)} \right\rfloor, \left\lfloor \frac{\Gamma_{k, \max}^v}{\delta_k^v} - \frac{\sigma_k^v}{\delta_k^v P B M_1 (M_1^2 - 1)} \right\rfloor \right\}, \quad (49)$$

$$N_{q, \max}^C = \begin{cases} \left\lfloor \frac{1}{2 \ln \rho_q} \ln \left(\frac{\psi_{q,2}^{\text{MRT}}}{\psi_{q,1}^{\text{MRT}}} (2^{R_{q, \min}} - 1) \right) \right\rfloor + 1, \text{MRT}, \\ \left\lfloor \frac{1}{2 \ln \rho_q} \ln \left(\frac{(2^{R_{q, \min}} - 1) \psi_{q,2}^{\text{ZF}}}{\psi_{q,1}^{\text{ZF}} + (2^{R_{q, \min}} - 1) \psi_{q,3}^{\text{ZF}}} \right) \right\rfloor + 1, \text{ZF}, \end{cases} \quad (50)$$

respectively, where $\psi_{q,1}^{\text{MRT}} = M_1 \beta_q^2 P^2 B L_t$, $\psi_{q,2}^{\text{MRT}} = (P \beta_q + \tilde{\sigma}_q) (L_t \tilde{\sigma}_q + M_1 \beta_q P B)$, $\psi_{q,1}^{\text{ZF}} = M_1 \beta_q^2 P^2 B (L_t - Q)$, $\psi_{q,2}^{\text{ZF}} = (P \beta_q + \tilde{\sigma}_q) (L_t \tilde{\sigma}_q + M_1 \beta_q P B)$, and $\psi_{q,3}^{\text{ZF}} = M_1 \beta_q^2 P^2 B$.

Proof: Firstly, it is obviously that when all the power and bandwidth are allocated to U_k^R , it can achieve the largest channel aging time under the target tracking conditions, i.e., $p_k = P$ and $B_k = B$. Then, substituting (28) into constraints C2 and C3, we have (49). Similarly, by substituting (44) into constraints C4 with assuming $p_0 B_0 = P B$, we have (50). ■

Theorem 4.2: If problem **P2** with the fixed N is feasible, its optimal solution can be obtained by successively solving the following two subproblems, i.e.,

$$\begin{aligned} \mathbf{P2} - \mathbf{A} : (\mathbf{p}^*, \mathbf{B}^*) &= \arg \max_{\mathbf{p}, \mathbf{B}} p_0 B_0 \\ &\text{s.t. C1} - \text{C3, C5, C7, C8, and (47), \end{aligned}$$

and

$$\begin{aligned} \mathbf{P2} - \mathbf{B} : \tilde{\mathbf{p}}^* &= \arg \max_{\tilde{\mathbf{p}}} \mathcal{R}(N, \mathbf{p}^*, \tilde{\mathbf{p}}, \mathbf{B}^*) \\ &\text{s.t. C4, C6, and C9, \end{aligned}$$

where \mathbf{p}^* and \mathbf{B}^* are obtained by solving problem **P2** – **A**.

Proof: Please refer to Appendix D. ■

C. Optimal Solution to Problem **P2** – **A**

In this part, we provide the optimal solution to problem **P2** – **A**.

With the derived CRLBs in (28), constraints C1, C2, and C3 can be equivalently rewritten as

$$p_k B_k \geq \tilde{\Gamma}_{k, N}^{\theta, v}, \quad 1 \leq k \leq K, \quad (51)$$

$$p_k B_k (B_k^2 - 1) \geq \tilde{\Gamma}_{k, N}^d, \quad 1 \leq k \leq K, \quad (52)$$

where

$$\tilde{\Gamma}_{k, N}^{\theta, v} = \max \left\{ \left\{ \frac{a_{k, n} \sigma_k^{\theta}}{(\Gamma_{k, \max}^{\theta} - b_{k, n} \delta_k^{\theta}) M_1}, \forall n \right\}, \frac{\sigma_k^v}{M_1 (M_1^2 - 1) (\Gamma_{k, \max}^v - (N - 1) \delta_k^v)} \right\}, \quad (53)$$

$$\tilde{\Gamma}_{k, N}^d = \frac{\sigma_k^d}{M_1 (\Gamma_{k, \max}^d - (N - 1) \delta_k^d)}. \quad (54)$$

Then, problem **P2** – **A** can be equivalently rewritten as

$$\mathbf{P2} - \mathbf{A1} : \max_{\mathbf{p}, \mathbf{B}} \ln(p_0) + \ln(B_0)$$

$$\text{s.t. } \ln(p_k) + \ln(B_k) \geq \ln(\tilde{\Gamma}_{k, N}^{\theta, v}), \quad 1 \leq k \leq K, \quad (55a)$$

$$\ln(p_k) + \ln(B_k) + \ln(B_k + 1)$$

$$+ \ln(B_k - 1) \geq \ln(\tilde{\Gamma}_{k, N}^d), \quad 1 \leq k \leq K, \quad (55b)$$

$$\text{C5, C7, C8, and (47),}$$

where constraints (55a) and (55b) are due to (51) and (52). It is straightforward to know that problem **P2** – **A1** is a convex optimization problem, and its optimal solution can be efficiently computed using the Matlab toolbox, i.e., CVX [45], which only has a polynomial time complexity.

D. Optimal Solution to **P2** – **B**

With the optimal p_0^* and B_0^* , it is straightforward to know that problem **P2** – **B** is a convex optimization problem. The optimal solutions are given in the following theorem.

Theorem 4.3: The optimal solutions $\tilde{\mathbf{p}}^*$ to problem **P2** – **B** is given by

$$\tilde{p}_{q, n}^* = p_{q, n}^{\min} + \max \left\{ 0, \frac{1}{\ln 2 \xi_n^*} - \frac{1 + \gamma_{q, n} p_{q, n}^{\min}}{\gamma_{q, n}} \right\}, \quad (56)$$

where $p_{q, n}^{\min} = \frac{1}{\gamma_{q, n}} \left(2^{\frac{M}{M_n} R_{q, \min}} - 1 \right)$ and $\gamma_{q, n}$ is given in (44) with setting $p_0 = p_0^*$ and $B_0 = B_0^*$. Furthermore, ξ_n^* is the water level, which can be found by utilizing enumeration and solving $\sum_{q=1}^Q \tilde{p}_{q, n} = P$ for $1 \leq n \leq N$.

Proof: This can be proved by using the standard Lagrange dual algorithm [46], which is omitted here for brevity. ■

Finally, the optimal solutions to problem **P2** can be obtained by finding the optimal N that makes the objective maximum. The overall one-dimensional search based optimization algorithm is summarized in Algorithm 1

Parameters	Value	Parameters	Value
Speed of light	$c_0 = 3 \times 10^8$ m/s	Number of subcarriers	$B = 64$
Total signal bandwidth	$B\Delta_f = 10$ MHz	Subcarrier Bandwidth	$\Delta_f = 156.25$ KHz
Elementary OFDM symbol duration	$T_o = 1/\Delta_f = 6.4$ us	Cyclic prefix duration	$T_{cp} = \frac{1}{4}T = 1.6$ us
Transmit OFDM symbol duration	$T = 8$ us	Number of symbols	$M = 700$

TABLE I: Simulation parameter setup

E. Integer Conversion

If we denote $(\mathbf{p}^\dagger, \mathbf{B}^\dagger, \tilde{\mathbf{p}}^\dagger, N^\dagger)$ as the optimal solutions of problem **P2**, the solution \mathbf{B}^\dagger may violate the integer requirement, i.e., C10, of the original problem **P1**. Hence, we need to convert \mathbf{B}^\dagger into a feasible integer solution. However, considering the integer conversion problem is a combinatorial optimization problem that is challenging to solve optimally. Therefore, we develop the following heuristic algorithm to obtain its suboptimal solution. From (28), we know that a larger bandwidth will cause a better tracking performance. Thus, the integer solution, denoted by B_k^\ddagger , should be larger than B_k^\dagger for $1 \leq k \leq K$. Hence, we have the following heuristic integer solution, i.e.,

$$B_k^\ddagger = \begin{cases} \lceil B_k^\dagger \rceil, & \text{if } 1 \leq k \leq K, \\ B - \sum_{k=1}^K \lceil B_k^\dagger \rceil, & \text{if } k = 0, \end{cases} \quad (57)$$

where $\lceil \cdot \rceil$ is the ceiling function.

Algorithm 1 One-dimensional search based optimization algorithm for problem **P2**

- 1: Calculate N_{\max} using (48)
 - 2: **for** channel aging time $N=1:1:N_{\max}$ **do**
 - 3: Solve **P2** – **A** and obtain $(\mathbf{p}^*, \mathbf{B}^*)$
 - 4: With the optimal p_0^* and B_0^* for the current N , solve **P2** – **B** and obtain $\mathcal{R}(N, \mathbf{p}^*, \tilde{\mathbf{p}}^*, \mathbf{B}^*)$
 - 5: **end for**
 - 6: Find $\mathcal{R}(N^\dagger, \mathbf{p}^\dagger, \tilde{\mathbf{p}}^\dagger, \mathbf{B}^\dagger) = \max_N \mathcal{R}(N, \mathbf{p}^*, \tilde{\mathbf{p}}^*, \mathbf{B}^*)$
-

V. SIMULATION RESULTS

In this section, we show simulation results to validate the analyzed theoretical results and the effectiveness of the proposed algorithm. Specifically, we consider the system is operated on carrier frequency of $f_c = 5.89$ GHz from IEEE 802.11p [47]. The large-scale effect of communication channel is modeled by $(74.24 + 16.1 \log_{10} d_q^C / d_o)$ [48], where $d_o = 1$ m is the reference distance and d_q^C is the distance between the BS and communication receiver U_q^C , which follows continuous and uniformly distribution over $[1.5, 4.5]$ km. The temporal correlation coefficient ρ_q is set as 0.96. The noise power spectral densities at the BS and receiver U_q^R are set as -174 dBm/Hz. The initial angle, distance, and velocity of U_k^R follow continuous and uniformly distribution over $[\frac{(k-1)\pi}{16}, \frac{k\pi}{16}]$ rad, $[15, 45]$ m/s, and $[0.1, 0.3]$ km, respectively. Moreover, the associate state evaluation noise powers are set as $\delta_k^\theta = 10^{-5}$ rad, $\delta_k^d = 0.2$ m, and $\delta_k^v = 0.1$ m/s, respectively. Besides, the corresponding maximum tracking errors are set as $\Gamma_{k,\max}^\theta = 15\delta_k^\theta$, $\Gamma_{k,\max}^d = 15\delta_k^d$, and $\Gamma_{k,\max}^v = 15\delta_k^v$. We assume a uniform reflectivity model is adopted for each radar

target and do not consider the specific RCSs for simplification [24], [49], i.e., $\sigma_{\text{RCS},k} = 1$ m². The minimum transmission rate of U_q^C is set as $\frac{1}{10} \log_2 \left(1 + \frac{P\beta_q}{\sigma_q Q} \right)$. Finally, we use the similar setup in [37] for the remaining parameters, as shown in Table I.

In the following simulations, we compare the system performances obtained from our proposed algorithm and the following baseline schemes. Note that the results of each method are averaged over 1000 Monte Carlo trials.

- Upper Bound: we obtain the optimal solution of the relaxed problem, **P2**, using the proposed algorithm, without taking into account the integer constraint C10. This relaxation allows us to obtain an upper bound that outperforms other algorithms.
- Benchmark 1: we search for all potential N , and each is with optimized power and bandwidth by solving **P2** – **A** in Phase-I and uniform power in the remaining data transmission.
- Benchmark 2: we search for all potential N , and each is with uniform power and bandwidth allocation in Phase-I, but the optimized power allocating using (56) in the remaining data transmission.
- Benchmark 3: we search for all potential N , and each is with uniform power and bandwidth for the entire transmission frame.
- Without Channel Aging: we use the proposed algorithm to solve the original problem by setting $N = 1$.

Fig. 4 shows the impact of maximum transmit power on the simulated and theoretical radar tracking performances, i.e., the root of mean square error (RMSE), when the uniform power and bandwidth allocation is applied in the whole frame without considering sensing and communication performance requirements. The RMSE is defined as $(\text{RMSE} = \sqrt{\frac{1}{K} \sum_{k=1}^K (x_k - \hat{x}_k)^2})$, where x_k and \hat{x}_k are the true and estimated parameters, respectively. From Fig. 4, we observe that the simulated RMSEs of the angle, distance, and velocity from (12), (15), and (16), can approach the theoretical results obtained by (18) when $N = 1$ and by (27) when $N = 10$, which validates the correctness of the analyzed radar channel estimation and prediction results. Also, we observe that the proposed approximated results in (28) can achieve nearly identical performances to the original theoretical results, which validates the effectiveness of the proposed approximation method. Finally, we note that the tracking performances decrease as the channel aging time increases. This is because a larger channel aging time introduces higher evaluation noise in the radar channel model, which leads to worse tracking performance.

Fig. 5 shows the impact of maximum transmit power on the simulated and theoretical communication performances. Here

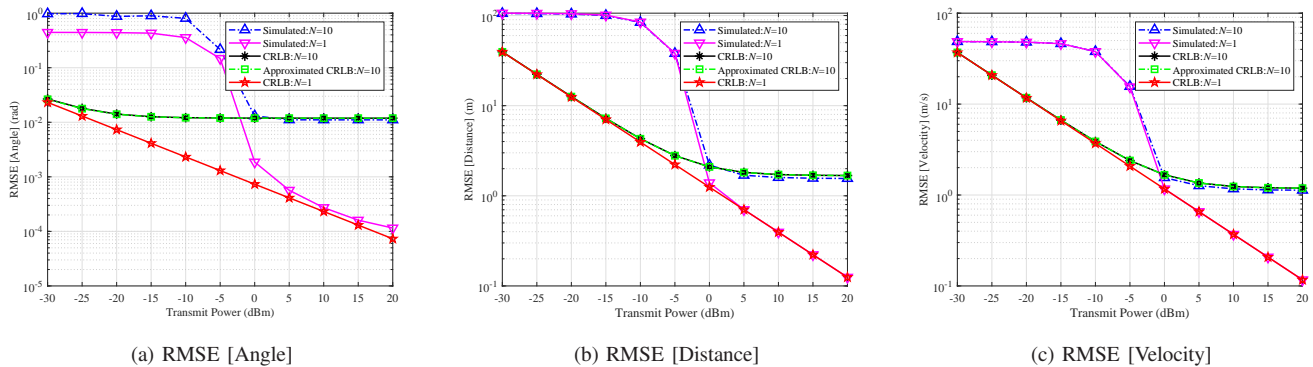


Fig. 4: The RMSEs versus the maximum transmit power with the uniform power and bandwidth allocation: $K = 4$, $M_1 = 60$, $L_t = 24$, and $L_r = 64$.

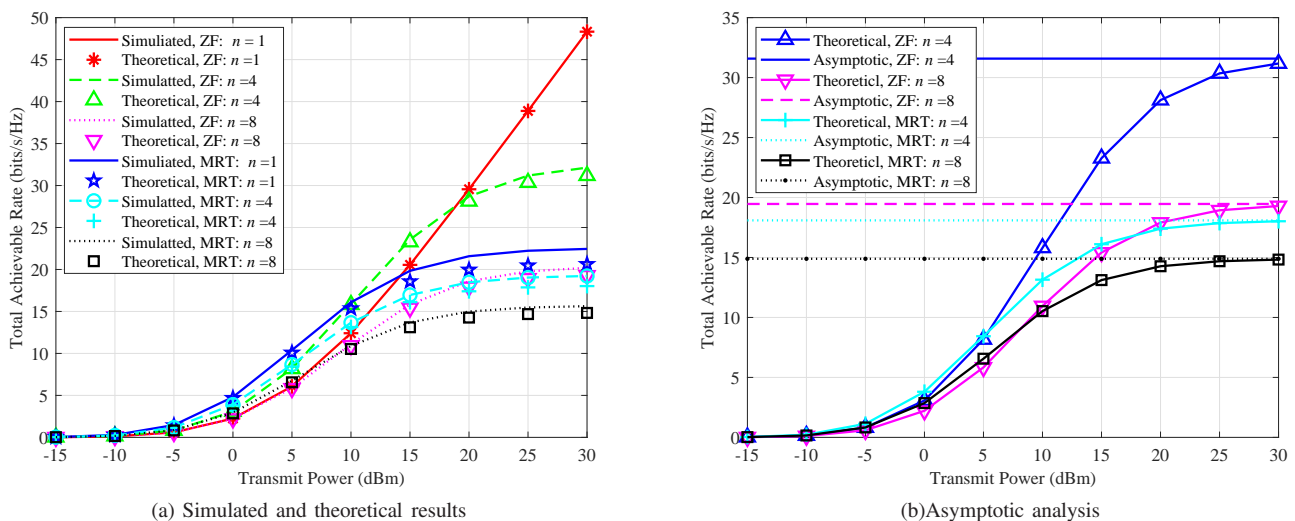


Fig. 5: The total achievable rate of all users in the n -th block versus the maximum transmit power with the uniform power and bandwidth allocation: $K = 4$, $Q = 10$, $M_1 = 300$, $L_t = 32$, and $L_r = 64$.

we consider the total achievable transmission rate in the n -th block, denoted as $R_n = \sum_{q=1}^Q R_{q,n}$, when uniform power and bandwidth allocation is applied for the entire transmission frame, without considering sensing and communication performance requirements. From Fig. 5(a), we observe that the theoretical total achievable rates obtained from (44) match the simulated results, which verifies the correctness of the derived theoretical results. Furthermore, we observe that the rates obtained using MRT for any N are bounded as power increases due to the existence of interference in the MRT scheme with non-orthogonal channels. In contrast, rates obtained using ZF are not bounded only when $N = 1$, since no interference exists in the ZF scheme. However, this does not hold when $N \geq 2$ due to the existence of channel evaluation noise. From Fig. 5(b), we observe that all results are bounded by the asymptotic results obtained in (45), which verifies the derived theoretical results.

Fig. 6 shows the impact of channel aging time on the average total achievable transmission rate. Note that in this figure, the channel aging time is a constant and does not need to be optimized in problem **P1**. Hence, the proposed algorithm and other benchmarks with minor modifications can be applied

to solve problem **P1** with a fixed N . From this figure, we observe that the performance of each scheme initially increases and then decreases with the channel aging time. This is because exploiting the channel aging effect reduces the training overhead in CSI estimation and radar target tracking, which results in an increase in the achievable rate. However, the powers of the evaluation noises of the aged communication and radar channels also increase with the channel aging time, ultimately leading to a decrease in the rate. This observation motivates us to determine the optimal channel aging time that satisfies the specific system requirements and user demands.

Fig. 7 shows the impact of maximum transmit power on the average total achievable transmission rate. From this figure, we can observe that the total achievable rate of each scheme increases with the transmit power. Besides, the proposed algorithm can achieve similar performance to the upper bound scheme and outperforms the baseline schemes, which demonstrates the effectiveness of the proposed algorithm. Moreover, the performance gap between the proposed algorithm and the "Without Channel Aging" scheme increases with the transmit power. The reason is that a better estimation/tracking performance can be obtained in the first block with a higher transmit

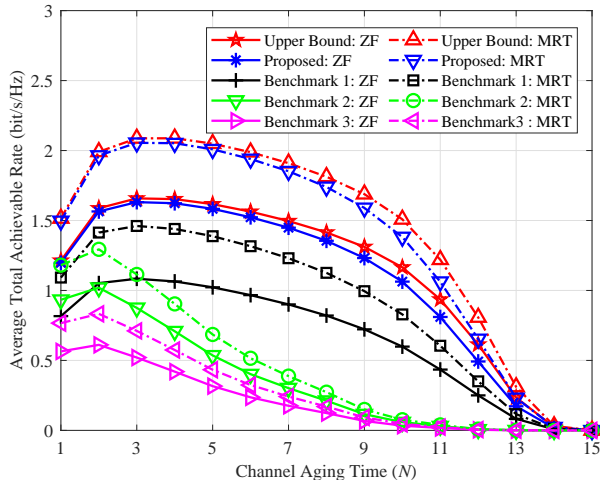


Fig. 6: The average total achievable rate versus the channel aging time: $P = -5$ dBm, $K = 4$, $Q = 10$, $M_1 = 300$, $L_t = 32$,

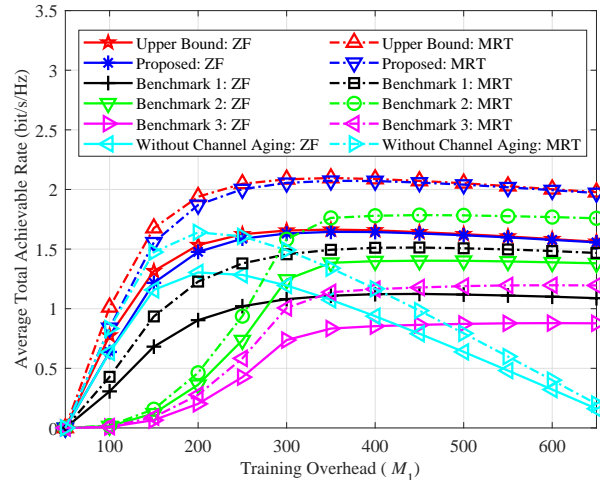


Fig. 8: The average total achievable rate versus the training overhead: $P = -5$ dBm, $K = 4$, $Q = 10$, $L_t = 32$, and $L_r = 64$.

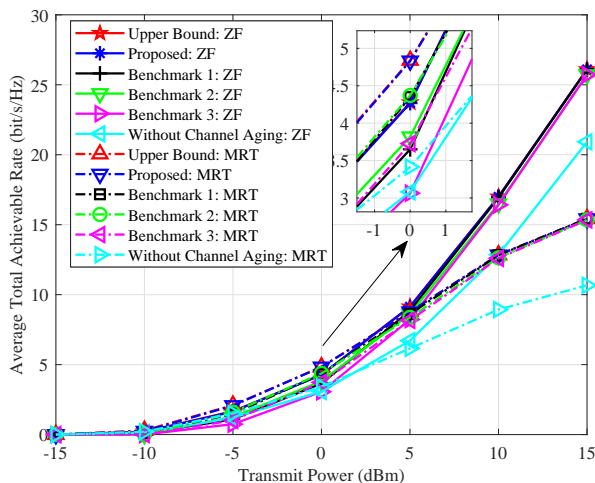


Fig. 7: The average total achievable rate versus the maximum transmit power: $K = 4$, $Q = 10$, $M_1 = 300$, $L_t = 32$, and $L_r = 64$.

power, thus causing a larger optimal channel aging time and higher transmission efficiency. These findings validate the importance of utilizing channel aging to improve system performance. Finally, it is observed that the algorithms with MRT beamforming outperform those with ZF beamforming in the low power region, but are inferior in the high power region. These results can guide the beamforming design for the studied system.

Fig. 8 shows the impact of training overhead on the average total achievable rate. It can be observed that the performance of each scheme increases initially and then decreases as the training overhead increases. The reason behind this is that a larger number of training signals can lead to better estimation/tracking performance, resulting in a higher achievable transmission rate. However, higher training overhead also implies less data transmission time in the first block, resulting in a lower achievable rate. Additionally, we can observe that the "Without Channel Aging" scheme's performance decreases

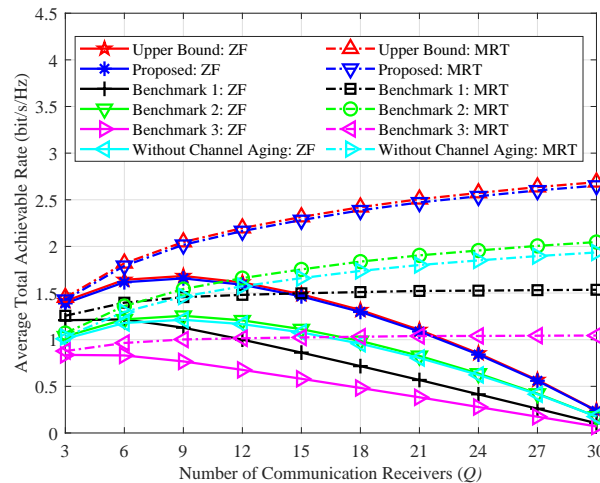


Fig. 9: The average total achievable rate versus the number of communication receivers: $P = -5$ dBm, $K = 4$, $M_1 = 300$, $L_t = 32$, and $L_r = 64$.

faster than other schemes. This is because the training overhead exists in each block for this scheme, while it only exists in the first block for other schemes. This highlights the significant benefits of optimizing channel aging time in the system design.

Fig. 9 shows the impact of the number of communication receivers on the average total achievable rate. From this figure, we observe that the performances of the MRT-based schemes increase with the number of users. Because a larger number of users provides a larger degree of freedom for system design, thus causing a higher achievable rate. However, the ZF-based schemes work worse with a larger number of users. This is because ZF-based schemes need to guarantee orthogonality among all users. Thus, given the number of transmit antennas, the beamforming gain of the ZF-based scheme decreases with the number of users, thus causing a lower rate. This can be applied to guide the beamforming design for the studied system.

VI. CONCLUSION

This paper leverages channel aging characteristics to reduce the training overhead and proposes a situation-dependent channel re-estimation interval optimization-based resource allocation scheme for a downlink multi-user/-target DFRC system. Specifically, we characterize the channel aging effects on the radar tracking CRLB performance and communication achievable rate performance, respectively. Then, these two performance metrics are derived as closed-form expressions with respect to the bandwidth, power, and channel aging time. Building on that, we formulate an average total aged achievable rate maximization problem subject to individual tracking precision demand, customized communication rate requirement, and other practical constraints. Moreover, the one-dimensional search based optimization algorithm is proposed to solve this problem efficiently. Finally, simulation results validate the correctness of the derived results and the effectiveness of the proposed algorithm.

APPENDIX

A. Proof of Theorem 3.1

To simplify the notations when deriving CRLB, we ignore the subscript k of $\bar{\mathbf{y}}_k^{\text{R}}(m, b)$ in (11) if there is no ambiguity and we denote the $(l+1)$ -th entry of vector $\bar{\mathbf{y}}_k^{\text{R}}(m, b)$ by $y_{m,b,l}$ for $0 \leq l \leq L_r - 1$. By denoting $\bar{\nu} = 2\pi T \nu^D$ and $\bar{\tau} = 2\pi \Delta_f \tau$ in (11), we have

$$y_{m,b,l} = \alpha e^{j(\phi - l\pi \sin(\theta) + b\bar{\tau} + m\bar{\nu})} + \omega_{m,b,l}, \quad (58)$$

where $\omega_{m,b,l}$ is the corresponding equivalent Gaussian noise with mean zero and variance $\frac{\sigma \Delta_f}{p L_t}$.

Then, by denoting $\mathbf{z} = [\theta, \bar{\tau}, \bar{\nu}, \alpha, \phi]^T$, we can obtain the corresponding fisher information matrix as

$$\mathbf{J}_{ij} = \frac{2pL_t}{\sigma \Delta_f} \sum_{m=0}^{M_1-1} \sum_{b=0}^{B_k-1} \sum_{l=0}^{L_r-1} \left[\frac{\partial y_{m,b,l}^{\text{Re}}}{\partial z_i} \frac{\partial y_{m,b,l}^{\text{Re}}}{\partial z_j} + \frac{\partial y_{m,b,l}^{\text{Im}}}{\partial z_i} \frac{\partial y_{m,b,l}^{\text{Im}}}{\partial z_j} \right], \quad (59)$$

where z_i is the i -th entry of vector \mathbf{z} with $1 \leq i \leq 5$, $y_{m,b,l}^{\text{Re}}$ and $y_{m,b,l}^{\text{Im}}$ are the real and imaginary components of $y_{m,b,l}$, respectively. Then, the bounds of the estimation error covariance are

$$\text{var}(\hat{z}_i) \geq \mathbf{J}^{-1}(i, i), \quad (60)$$

where $\mathbf{J}^{-1}(i, i)$ is the i -th diagonal element of the inverse matrix \mathbf{J} .

Since it is quite difficult to derive the closed-form bounds from (60) by using all the measurements due to the complexity of inverse processing, we use the similar method in [42] to obtain a simpler lower bound. For calculating the bound of θ , we can use the fact that each measurement has a different, random, and unknown initial phase due to the unknown Doppler shift and time delay. Since the white noise is assumed as the source of error, the estimation of θ from each measurement can be regarded as independent [42]. By applying the probability theory, we have

$$\text{var}(\hat{\theta}) \geq \frac{1}{M_1 B_k} \mathbf{J}_{\theta}^{-1}(1, 1), \quad (61)$$

where $\mathbf{J}_{\theta} = \frac{2pL_t}{\sigma \Delta_f} \sum_{l=0}^{L_r-1} \left[\frac{\partial y_{m,b,l}^{\text{Re}}}{\partial z_i} \frac{\partial y_{m,b,l}^{\text{Re}}}{\partial z_j} + \frac{\partial y_{m,b,l}^{\text{Im}}}{\partial z_i} \frac{\partial y_{m,b,l}^{\text{Im}}}{\partial z_j} \right]$, $i, j \in \{1, 4, 5\}$. Substituting (58) into (61), we have

$$\text{var}(\hat{\theta}) \geq \frac{6\sigma \Delta_f}{p |\alpha|^2 \pi^2 \cos^2(\theta) B_k M_1 L_t L_r (L_r^2 - 1)}. \quad (62)$$

Similarly, we can define $\mathbf{J}_{\bar{\tau}} = \frac{2pL_t}{\sigma \Delta_f} \sum_{b=0}^{B_k-1} \left[\frac{\partial y_{m,b,l}^{\text{Re}}}{\partial z_i} \frac{\partial y_{m,b,l}^{\text{Re}}}{\partial z_j} + \frac{\partial y_{m,b,l}^{\text{Im}}}{\partial z_i} \frac{\partial y_{m,b,l}^{\text{Im}}}{\partial z_j} \right]$, $i, j \in \{2, 4, 5\}$ and $\mathbf{J}_{\bar{\nu}} = \frac{2pL_t}{\sigma \Delta_f} \sum_{m=0}^{M_1-1} \left[\frac{\partial y_{m,b,l}^{\text{Re}}}{\partial z_i} \frac{\partial y_{m,b,l}^{\text{Re}}}{\partial z_j} + \frac{\partial y_{m,b,l}^{\text{Im}}}{\partial z_i} \frac{\partial y_{m,b,l}^{\text{Im}}}{\partial z_j} \right]$, $i, j \in \{3, 4, 5\}$ to derive the bounds of $\bar{\tau}$ and $\bar{\nu}$, respectively, and then we have

$$\text{var}(\hat{\bar{\tau}}) \geq \frac{6\sigma \Delta_f}{p |\alpha|^2 B_k M_1 L_t L_r (B_k^2 - 1)}, \quad (63)$$

$$\text{var}(\hat{\bar{\nu}}) \geq \frac{6\sigma \Delta_f}{p |\alpha|^2 B_k M_1 L_t L_r (M_1^2 - 1)}. \quad (64)$$

Then, since $\bar{\tau} = 2\pi \Delta_f \tau$ and $\tau = 2 \frac{d}{c_0}$, we have $\bar{\tau} = 4\pi \Delta_f \frac{d}{c_0}$. Also, since $\bar{\nu} = 2\pi T \nu^D$ and $\nu^D = \frac{2v \cos(\theta - \varphi_k)}{c_0} f_c$, we have $\bar{\nu} = 4\pi T f_c \frac{v \cos(\theta - \varphi_k)}{c_0}$. Finally, based on the bounds derived in (63) and (64), we can obtain the CRLBs of distance d and velocity v as

$$\text{var}(\hat{d}) \geq \frac{3c_0^2 \sigma \Delta_f}{8(\pi \Delta_f)^2 p |\alpha|^2 B_k M_1 L_t L_r (B_k^2 - 1)}, \quad (65)$$

$$\text{var}(\hat{v}) \geq \frac{3c_0^2 \sigma \Delta_f}{8(\pi T)^2 f_c^2 p |\alpha|^2 \cos^2(\theta - \varphi_k) B_k M_1 L_t L_r (M_1^2 - 1)}. \quad (66)$$

B. Proof of Theorem 3.2

To simplify the notations when deriving the approximated CRLBs, we ignore the subscript k of all variables if there is no ambiguity. To begin with, the Jacobian matrix for $\partial \mathcal{G}(\mathbf{x})$ is defined as $\mathbf{G}_n = \frac{\partial \mathcal{G}(\mathbf{x})}{\partial \mathbf{x}} \big|_{\mathbf{x}=\hat{\mathbf{x}}_n}$. With (5) and (6), the Jacobian matrix \mathbf{G}_n can be calculated as

$$\mathbf{G}_n = \begin{bmatrix} 1 + \frac{\hat{v}_n \tilde{T}}{d_n} \cos(\hat{\theta}_n) & -\frac{\hat{v}_n \tilde{T}}{d_n^2} \sin(\hat{\theta}_n) & \frac{\tilde{T}}{d_n} \sin(\hat{\theta}_n) \\ \hat{v}_n \tilde{T} \sin(\hat{\theta}_n) & 1 & -\tilde{T} \cos(\hat{\theta}_n) \\ 0 & 0 & 1 \end{bmatrix}, \quad (67)$$

where $\hat{\theta}_n = \hat{\theta}_n - \varphi_k$. Since $\frac{\hat{v}_n \hat{v}_{n-1} \tilde{T}^2}{d_n d_{n-1}} \approx 0$, $\frac{\hat{v}_n \tilde{T}}{d_n^2} \approx 0$, and $\frac{\hat{v}_n \hat{v}_{n-1} \tilde{T}^2}{d_n} \approx 0$, $\mathbf{G}_n \mathbf{G}_{n-1}$ can be approximated by

$$\mathbf{G}_n \mathbf{G}_{n-1} \approx \begin{bmatrix} 1 + \sum_{i=n-1}^n \frac{\hat{v}_i \tilde{T}}{d_i} \cos(\hat{\theta}_i) & 0 & \sum_{i=n-1}^n \frac{\tilde{T}}{d_i} \sin(\hat{\theta}_i) \\ \sum_{i=n-1}^n \hat{v}_i \tilde{T} \sin(\hat{\theta}_i) & 1 & -\sum_{i=n-1}^n \tilde{T} \cos(\hat{\theta}_i) \\ 0 & 0 & 1 \end{bmatrix}. \quad (68)$$

Then, by some algebraic manipulations with utilizing (68), we have

$$\prod_{i'=i}^{n-1} \mathbf{G}_{i'} \approx \begin{bmatrix} 1 + \sum_{i'=i}^{n-1} \frac{\hat{v}_{i'} \tilde{T}}{d_{i'}} \cos(\hat{\theta}_{i'}) & 0 & \sum_{i'=i}^{n-1} \frac{\tilde{T}}{d_{i'}} \sin(\hat{\theta}_{i'}) \\ \sum_{i'=i}^{n-1} \hat{v}_{i'} \tilde{T} \sin(\hat{\theta}_{i'}) & 1 & -\sum_{i'=i}^{n-1} \tilde{T} \cos(\hat{\theta}_{i'}) \\ 0 & 0 & 1 \end{bmatrix}. \quad (69)$$

Similarly, due to $\frac{\hat{v}_i \hat{v}_{i'} \tilde{T}^2}{\hat{d}_i \hat{d}_{i'}} \approx 0$ for $i \neq i'$, the first and second terms of the right hand side of (26) can be approximated as the following two equations, respectively, i.e.,

$$\text{diag} \left(\tilde{\mathbf{G}}_{n-1} \mathbf{D} \tilde{\mathbf{G}}_{n-1}^H \right) \approx \text{diag} (a_n, 1, 1) \mathbf{D}, \quad (70)$$

$$\text{diag} \left(\sum_{i=1}^{n-1} \tilde{\mathbf{G}}_{n,i} \Sigma_\omega \tilde{\mathbf{G}}_{n,i}^H \right) \approx (n-1) \text{diag} \left(\frac{b_n}{n-1}, 1, 1 \right) \Sigma_\omega, \quad (71)$$

where $a_n = \left| 1 + \sum_{i=1}^{n-1} \frac{\hat{v}_i \tilde{T}}{\hat{d}_i} \cos(\hat{\theta}_i) \right|^2$ and $b_n = 1 + \sum_{i=2}^{n-1} \left| 1 + \sum_{i'=i}^{n-1} \frac{\hat{v}_{i'} \tilde{T}}{\hat{d}_{i'}} \cos(\hat{\theta}_{i'}) \right|^2$.

Finally, substituting (70) and (71) into (26), the CRLBs derived in (27) can be approximated as (28) and the proof is completed.

C. Proof of Theorem 3.3

When the MRT beamforming is applied, we have $\mathbf{f}_{q,n} = \frac{1}{\sqrt{\lambda_q L_t}} \hat{\mathbf{h}}_{q,1}$. Then, we have the following terms:

$$\begin{aligned} & \left| \mathbb{E} \left(\mathbf{h}_{q,n}^H \mathbf{f}_{q,n} \right) \right|^2 \\ &= \left| \mathbb{E} \left(\left(\hat{\mathbf{h}}_{q,n}^H + \bar{\mathbf{e}}_{q,n}^H \right) \frac{1}{\sqrt{\lambda_q L_t}} \hat{\mathbf{h}}_{q,1} \right) \right|^2 = \left| \mathbb{E} \left(\frac{\rho_q^{n-1}}{\sqrt{\lambda_q L_t}} \hat{\mathbf{h}}_{q,1}^H \hat{\mathbf{h}}_{q,1} \right) \right|^2 \\ &= \rho_q^{2(n-1)} \lambda_q L_t, \end{aligned} \quad (72)$$

$$\begin{aligned} & \mathbb{E} \left(\left| \mathbf{h}_{q,n}^H \mathbf{f}_{q,n} - \mathbb{E} \left(\mathbf{h}_{q,n}^H \mathbf{f}_{q,n} \right) \right|^2 \right) \\ &= \mathbb{E} \left(\left| \frac{\rho_q^{n-1}}{\sqrt{\lambda_q L_t}} \hat{\mathbf{h}}_{q,1}^H \hat{\mathbf{h}}_{q,1} \right|^2 \right) + \mathbb{E} \left(\left| \frac{1}{\sqrt{\lambda_q L_t}} \bar{\mathbf{e}}_{q,n}^H \hat{\mathbf{h}}_{q,1} \right|^2 \right) - \left| \mathbb{E} \left(\mathbf{h}_{q,n}^H \mathbf{f}_{q,n} \right) \right|^2 \\ &= \rho_q^{2(n-1)} \lambda_q (L_t + 1) + (\beta_q - \rho_q^{2(n-1)} \lambda_q) - \rho_q^{2(n-1)} \lambda_q L_t = \beta_q, \end{aligned} \quad (73)$$

$$\begin{aligned} & \mathbb{E} \left(\left| \left(\hat{\mathbf{h}}_{q,n}^H + \bar{\mathbf{e}}_{q,n}^H \right) \mathbf{f}_{i,n} \right|^2 \right) \\ &= \mathbb{E} \left(\left| \frac{\rho_q^{n-1}}{\sqrt{\lambda_i L_t}} \hat{\mathbf{h}}_{q,1}^H \hat{\mathbf{h}}_{i,1} \right|^2 \right) + \mathbb{E} \left(\left| \frac{1}{\sqrt{\lambda_i L_t}} \bar{\mathbf{e}}_{q,n}^H \hat{\mathbf{h}}_{i,1} \right|^2 \right) \\ &= \rho_q^{2(n-1)} \lambda_q + (\beta_q - \rho_q^{2(n-1)} \lambda_q) = \beta_q. \end{aligned} \quad (74)$$

Then, by substituting (72), (73), and (74) into (42), the channel-to-interference-plus-noise ratio $\gamma_{q,n}$ under MRT is given in (44).

When the ZF beamforming is applied, we have $\mathbf{f}_{q,n} = \sqrt{\lambda_q} (L_t - Q) \mathbf{a}_q$. According to [44], $\hat{\mathbf{h}}_{q,1}^H \mathbf{a}_i = 1$ if $q = i$, and 0 otherwise. Then, we can derive the following terms:

$$\begin{aligned} & \left| \mathbb{E} \left(\mathbf{h}_{q,n}^H \mathbf{f}_{q,n} \right) \right|^2 \\ &= \left| \mathbb{E} \left(\left(\hat{\mathbf{h}}_{q,n}^H + \bar{\mathbf{e}}_{q,n}^H \right) \sqrt{\lambda_q (L_t - Q)} \mathbf{a}_q \right) \right|^2 = \rho_q^{2(n-1)} \lambda_q (L_t - Q), \end{aligned} \quad (75)$$

$$\begin{aligned} & \mathbb{E} \left(\left| \mathbf{h}_{q,n}^H \mathbf{f}_n - \mathbb{E} \left(\mathbf{h}_{q,n}^H \mathbf{f}_n \right) \right|^2 \right) \\ &= \mathbb{E} \left(\left| \left(\rho_q^{n-1} \hat{\mathbf{h}}_{q,1}^H + \bar{\mathbf{e}}_{q,n}^H \right) \sqrt{\lambda_q (L_t - Q)} \mathbf{a}_q \right|^2 \right) - \left| \mathbb{E} \left(\mathbf{h}_{q,n}^H \mathbf{f}_{q,n} \right) \right|^2 \\ &= \lambda_q (L_t - Q) (\beta_q - \rho_q^{2(n-1)} \lambda_q) \mathbb{E} \left(\|\mathbf{a}_q\|^2 \right) = \beta_q - \rho_q^{2(n-1)} \lambda_q, \end{aligned} \quad (76)$$

$$\begin{aligned} & \mathbb{E} \left(\left| \left(\hat{\mathbf{h}}_{q,n}^H + \bar{\mathbf{e}}_{q,n}^H \right) \mathbf{f}_{i,n} \right|^2 \right) \\ &= \mathbb{E} \left(\left| \rho_q^{n-1} \hat{\mathbf{h}}_{q,1}^H \sqrt{\lambda_i (L_t - Q)} \mathbf{a}_i \right|^2 \right) + \mathbb{E} \left(\left| \bar{\mathbf{e}}_{q,n}^H \sqrt{\lambda_i (L_t - Q)} \mathbf{a}_i \right|^2 \right) \\ &= \beta_q - \rho_q^{2(n-1)} \lambda_q. \end{aligned} \quad (77)$$

Finally, by substituting (75), (76), and (77) into (42), the channel-to-interference-plus-noise ratio $\gamma_{q,n}$ under ZF is given in (44). Finally, the proof is completed.

D. Proof of Theorem 4.2

For notation simplicity in the following proof, the objective function $\mathcal{R}(N, \mathbf{p}, \tilde{\mathbf{p}}, \mathbf{B})$ with fixed N can be expressed as the function $F(p_0 B_0, \tilde{\mathbf{p}})$, which is only dependent on $p_0 B_0$ and $\tilde{\mathbf{p}}$. In the following, we apply the contradiction method to prove the transform equivalence.

Firstly, since problem **P2** with the fixed N is feasible, we assume that $\mathbf{p}^* = [p_0^*, p_1^*, \dots, p_K^*]^T$ and $\mathbf{B}^* = [B_0^*, B_1^*, \dots, B_K^*]^T$ are the corresponding optimal solutions.

Also, we assume that $\mathbf{p}^\dagger = [p_0^\dagger, p_1^\dagger, \dots, p_K^\dagger]^T$ and $\mathbf{B}^\dagger =$

$[B_0^\dagger, B_1^\dagger, \dots, B_K^\dagger]^T$ are the optimal solutions to problem **P2** – **A** with the same fixed N . Based on the above assumptions, we know \mathbf{p}^\dagger , \mathbf{B}^\dagger , and $\tilde{\mathbf{p}}^*$ are also the feasible solutions of problem **P2** with the fixed N . Besides, we have the following important results based on the above assumptions, i.e., $F(p_0^* B_0^*, \tilde{\mathbf{p}}^*) \geq F(p_0^\dagger B_0^\dagger, \tilde{\mathbf{p}}^*)$ and $p_0^* B_0^* \leq p_0^\dagger B_0^\dagger$. However, it is straightforward to know that $F(p_0 B_0, \tilde{\mathbf{p}})$ is a monotonic increasing function with respect to $p_0 B_0$. Thus, if $p_0^* B_0^* \leq p_0^\dagger B_0^\dagger$, we have $F(p_0^* B_0^*, \tilde{\mathbf{p}}^*) \leq F(p_0^\dagger B_0^\dagger, \tilde{\mathbf{p}}^*)$. This contradicts with the assumption that p_0^* and B_0^* are the optimal solutions to problem **P2** with the fixed N . Hence, we know problems **P2** and **P2** – **A** have the same solutions of \mathbf{p} and \mathbf{B} . Recalling that $F(p_0 B_0, \tilde{\mathbf{p}})$ is only dependent on $p_0 B_0$ and $\tilde{\mathbf{p}}$. Thus, once $p_0 B_0$ is obtained, it is straightforward to know that the optimal $\tilde{\mathbf{p}}$ of problem **P2** can be obtained by solving problem **P2** – **B**. Hence, the theorem is proved.

REFERENCES

- [1] L. Zheng, M. Lops, Y. C. Eldar, and X. Wang, "Radar and communication coexistence: An overview: A review of recent methods," *IEEE Signal Process. Mag.*, vol. 36, no. 5, pp. 85–99, 2019.
- [2] F. Liu, Y. Cui, C. Masouros, J. Xu, T. X. Han, Y. C. Eldar, and S. Buzzi, "Integrated sensing and communications: Towards dual-functional wireless networks for 6G and beyond," *IEEE J. Sel. Areas Commun.*, vol. 40, no. 6, pp. 1728–1767, 2022.
- [3] C. Sturm and W. Wiesbeck, "Waveform design and signal processing aspects for fusion of wireless communications and radar sensing," *Proc. IEEE*, vol. 99, no. 7, pp. 1236–1259, 2011.
- [4] F. Liu, C. Masouros, A. P. Petropulu, H. Griffiths, and L. Hanzo, "Joint radar and communication design: Applications, state-of-the-art, and the road ahead," *IEEE Trans. Commun.*, vol. 68, no. 6, pp. 3834–3862, 2020.
- [5] H. Yang, Z. Wei, Z. Feng, C. Qiu, Z. Fang, X. Chen, and P. Zhang, "Queue-aware dynamic resource allocation for the joint communication-radar system," *IEEE Trans. Veh. Technol.*, vol. 70, no. 1, pp. 754–767, 2020.
- [6] C. Ouyang, Y. Liu, and H. Yang, "NOMA-ISAC: Performance analysis and rate region characterization," *arXiv preprint arXiv:2205.13756*, 2022.
- [7] T. Tian, G. Li, H. Deng, and J. Lu, "Adaptive bit/power allocation with beamforming for dual-function radar-communication," *IEEE Wireless Commun. Lett.*, vol. 11, no. 6, pp. 1186–1190, Jun. 2022.
- [8] M. Temiz, E. Alsusa, and M. W. Baidas, "Optimized precoders for massive MIMO OFDM dual radar-communication systems," *IEEE Trans. Commun.*, vol. 69, no. 7, pp. 4781–4794, 2021.
- [9] Y. Luo, J. A. Zhang, X. Huang, W. Ni, and J. Pan, "Optimization and quantization of multibeam beamforming vector for joint communication and radio sensing," *IEEE Trans. Commun.*, vol. 67, no. 9, pp. 6468–6482, 2019.

- [10] X. Zhou, L. Tang, Y. Bai, and Y.-C. Liang, "Performance analysis and waveform optimization of integrated FD-MIMO radar-communication systems," *IEEE Trans. Wireless Commun.*, vol. 20, no. 11, pp. 7490–7502, 2021.
- [11] X. Wang, Z. Fei, J. A. Zhang, J. Huang, and J. Yuan, "Constrained utility maximization in dual-functional radar-communication multi-UAV networks," *IEEE Trans. Commun.*, vol. 69, no. 4, pp. 2660–2672, 2020.
- [12] Z. Wang, Y. Liu, X. Mu, and Z. Ding, "NOMA inspired interference cancellation for integrated sensing and communication," in *Proc. IEEE Inter. Conf. Commun. (ICC)*, 2022, pp. 3154–3159.
- [13] M. Ashraf and B. Tan, "Detection probability maximization scheme in integrated sensing and communication systems," in *Proc. IEEE Veh. Technol. Conf. (VTC-Spring)*, 2022, pp. 1–6.
- [14] G. Cui, H. Li, and M. Rangaswamy, "MIMO radar waveform design with constant modulus and similarity constraints," *IEEE Trans. Signal Process.*, vol. 62, no. 2, pp. 343–353, 2013.
- [15] M. Hua, Q. Wu, W. Chen, and A. Jamalipour, "Integrated sensing and communication: Joint pilot and transmission design," *arXiv preprint arXiv:2211.12891*, 2022.
- [16] N. Cao, Y. Chen, X. Gu, and W. Feng, "Joint radar-communication waveform designs using signals from multiplexed users," *IEEE Trans. Commun.*, vol. 68, no. 8, pp. 5216–5227, 2020.
- [17] Z. Ni, J. A. Zhang, K. Yang, X. Huang, and T. A. Tsiftsis, "Multi-metric waveform optimization for multiple-input single-output joint communication and radar sensing," *IEEE Trans. Commun.*, vol. 70, no. 2, pp. 1276–1289, 2021.
- [18] M. Xie, W. Yi, T. Kirubarajan, and L. Kong, "Joint node selection and power allocation strategy for multitarget tracking in decentralized radar networks," *IEEE Trans. Signal Process.*, vol. 66, no. 3, pp. 729–743, 2017.
- [19] X. Yuan, Z. Feng, J. A. Zhang, W. Ni, R. P. Liu, Z. Wei, and C. Xu, "Spatio-temporal power optimization for MIMO joint communication and radio sensing systems with training overhead," *IEEE Trans. Veh. Technol.*, vol. 70, no. 1, pp. 514–528, 2020.
- [20] P. Kumari, S. A. Vorobyov, and R. W. Heath, "Adaptive virtual waveform design for millimeter-wave joint communication–radar," *IEEE Trans. Signal Process.*, vol. 68, pp. 715–730, 2019.
- [21] M. Hua, Q. Wu, C. He, S. Ma, and W. Chen, "Joint active and passive beamforming design for IRS-aided radar-communication," *IEEE Trans. Wireless Commun.*, pp. 1–1, 2022, doi: 10.1109/TWC.2022.3210532.
- [22] J. Yan, H. Liu, B. Jiu, B. Chen, Z. Liu, and Z. Bao, "Simultaneous multibeam resource allocation scheme for multiple target tracking," *IEEE Trans. Signal Process.*, vol. 63, no. 12, pp. 3110–3122, 2015.
- [23] J. Yan, H. Liu, B. Jiu, and Z. Bao, "Power allocation algorithm for target tracking in unmodulated continuous wave radar network," *IEEE Sens. J.*, vol. 15, no. 2, pp. 1098–1108, 2014.
- [24] H. Zhang, B. Zong, and J. Xie, "Power and bandwidth allocation for multi-target tracking in collocated MIMO radar," *IEEE Trans. Veh. Technol.*, vol. 69, no. 9, pp. 9795–9806, 2020.
- [25] G. R. Muns, K. V. Mishra, C. B. Guerra, Y. C. Eldar, and K. R. Chowdhury, "Beam alignment and tracking for autonomous vehicular communication using IEEE 802.11 ad-based radar," in *Proc. IEEE Conf. Comput. Commun. Workshops (INFOCOMWKSHPS)*, 2019, pp. 535–540.
- [26] W. Yuan, F. Liu, C. Masouros, J. Yuan, D. W. K. Ng, and N. González-Prelcic, "Bayesian predictive beamforming for vehicular networks: A low-overhead joint radar-communication approach," *IEEE Trans. Wireless Commun.*, vol. 20, no. 3, pp. 1442–1456, 2020.
- [27] F. Liu, W. Yuan, C. Masouros, and J. Yuan, "Radar-assisted predictive beamforming for vehicular links: Communication served by sensing," *IEEE Trans. Wireless Commun.*, vol. 19, no. 11, pp. 7704–7719, 2020.
- [28] C. Liu, W. Yuan, S. Li, X. Liu, H. Li, D. W. K. Ng, and Y. Li, "Learning-based predictive beamforming for integrated sensing and communication in vehicular networks," *IEEE J. Sel. Areas Commun.*, vol. 40, no. 8, pp. 2317–2334, 2022.
- [29] Y. Zhou, P. C. Yip, and H. Leung, "Tracking the direction-of-arrival of multiple moving targets by passive arrays: Algorithm," *IEEE Trans. Signal Process.*, vol. 47, no. 10, pp. 2655–2666, 1999.
- [30] P. Chen, C. Qi, L. Wu, and X. Wang, "Waveform design for kalman filter-based target scattering coefficient estimation in adaptive radar system," *IEEE Trans. Veh. Technol.*, vol. 67, no. 12, pp. 11 805–11 817, 2018.
- [31] K. E. Baddour and N. C. Beaulieu, "Autoregressive modeling for fading channel simulation," *IEEE Trans. Wireless Commun.*, vol. 4, no. 4, pp. 1650–1662, 2005.
- [32] R. Chopra, C. R. Murthy, and H. A. Suraweera, "On the throughput of large MIMO beamforming systems with channel aging," *IEEE Signal Process. Lett.*, vol. 23, no. 11, pp. 1523–1527, 2016.
- [33] C. Kong, C. Zhong, A. K. Papazafeiropoulos, M. Matthaiou, and Z. Zhang, "Sum-rate and power scaling of massive MIMO systems with channel aging," *IEEE Trans. Commun.*, vol. 63, no. 12, pp. 4879–4893, 2015.
- [34] A. K. Papazafeiropoulos, "Impact of general channel aging conditions on the downlink performance of massive MIMO," *IEEE Trans. Veh. Technol.*, vol. 66, no. 2, pp. 1428–1442, Feb. 2016.
- [35] R. Deng, Z. Jiang, S. Zhou, and Z. Niu, "Intermittent CSI update for massive MIMO systems with heterogeneous user mobility," *IEEE Trans. Commun.*, vol. 67, no. 7, pp. 4811–4824, 2019.
- [36] J. Zheng, J. Zhang, E. Björnson, and B. Ai, "Impact of channel aging on cell-free massive MIMO over spatially correlated channels," *IEEE Trans. Wireless Commun.*, vol. 20, no. 10, pp. 6451–6466, 2021.
- [37] L. Gaudio, M. Kobayashi, B. Bissinger, and G. Caire, "Performance analysis of joint radar and communication using OFDM and OTFS," in *Proc. Proc. IEEE Inter. Conf. Commun. Workshops (ICC Workshops)*, 2019, pp. 1–6.
- [38] H. Schober and F. Jondral, "Velocity estimation for OFDM based communication systems," in *Proc. IEEE Veh. Technol. Conf.*, vol. 2. IEEE, 2002, pp. 715–718.
- [39] L. G. de Oliveira, B. Nuss, M. B. Alabd, A. Diewald, M. Pauli, and T. Zwick, "Joint radar-communication systems: Modulation schemes and system design," *IEEE Trans. Microw. Theory Tech.*, vol. 70, no. 3, pp. 1521–1551, 2021.
- [40] L. Gaudio, M. Kobayashi, G. Caire, and G. Colavolpe, "On the effectiveness of OTFS for joint radar parameter estimation and communication," *IEEE Trans. Wireless Commun.*, vol. 19, no. 9, pp. 5951–5965, 2020.
- [41] J. Chen, Y.-C. Liang, H. V. Cheng, and W. Yu, "Channel estimation for reconfigurable intelligent surface aided multi-user mmwave MIMO systems," *IEEE Trans. Wireless Commun.*, pp. 1–1, 2023, doi: 10.1109/TWC.2023.3246264.
- [42] K. M. Braun, "OFDM radar algorithms in mobile communication networks," Ph.D. dissertation, Karlsruhe, Karlsruher Institut für Technologie (KIT), Diss., 2014, 2014.
- [43] S. M. Kay, *Fundamentals of statistical signal processing: estimation theory*. vol. 1. Englewood Cliffs, NJ, USA: Prentice-Hall., 1998.
- [44] H. Q. Ngo, E. G. Larsson, and T. L. Marzetta, "Energy and spectral efficiency of very large multiuser MIMO systems," *IEEE Trans. Commun.*, vol. 61, no. 4, pp. 1436–1449, 2013.
- [45] M. Grant, S. Boyd, and Y. Ye, "CVX: MATLAB software for disciplined convex programming," [Online]. Available: <http://stanford.edu/~boyd/cvx>.
- [46] J. Chen, L. Zhang, Y.-C. Liang, X. Kang, and R. Zhang, "Resource allocation for wireless-powered IoT networks with short packet communication," *IEEE Trans. Wireless Commun.*, vol. 18, no. 2, pp. 1447–1461, 2019.
- [47] D. H. Nguyen and R. W. Heath, "Delay and doppler processing for multi-target detection with IEEE 802.11 OFDM signaling," in *Proc. Int. Conf. Acoust. Speech Signal Process. (ICASSP)*, 2017, pp. 3414–3418.
- [48] O. Onubogu, K. Ziri-Castro, D. Jayalath, K. Ansari, and H. Suzuki, "Empirical vehicle-to-vehicle pathloss modeling in highway, suburban and urban environments at 5.8 ghz," in *Proc. Int. Conf. Signal Process. Commun. Syst. (ICSPCS)*. IEEE, 2014, pp. 1–6.
- [49] H. Godrich, A. P. Petropulu, and H. V. Poor, "Power allocation strategies for target localization in distributed multiple-radar architectures," *IEEE Trans. Signal Process.*, vol. 59, no. 7, pp. 3226–3240, 2011.